JCI insight

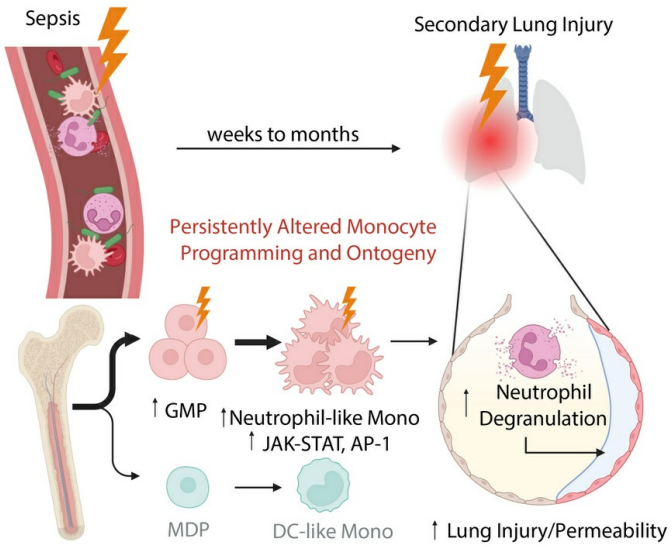
Long-term reprogramming of classical monocytes with altered ontogeny mediates enhanced lung injury in sepsis survivors

Scott J. Denstaedt, Breanna McBean, Alan P. Boyle, Brett C. Arenberg, Matthias Mack, Bethany B. Moore, Michael W. Newstead, Yamei Deng, Alexey I. Nesvizhskii, Benjamin H. Singer, Jennifer Cano, Hallie C. Prescott, Helen S. Goodridge, Rachel L. Zemans

JCI Insight. 2026;11(21):e198551. https://doi.org/10.1172/jci.insight.198551.

Research Article | Immunology | Infectious disease | Pulmonology

Graphical abstract



Find the latest version:

https://jci.me/198551/pdf

JCI insight

RESEARCH ARTICLE

Long-term reprogramming of classical monocytes with altered ontogeny mediates enhanced lung injury in sepsis survivors

Scott J. Denstaedt,[1] Breanna McBean,[2,3] Alan P. Boyle,[2,3] Brett C. Arenberg,[1] Matthias Mack,[4] Bethany B. Moore,[1,5] Michael W. Newstead,[1] Yamei Deng,[6] Alexey I. Nesvizhskii,[6,7] Benjamin H. Singer,[1] Jennifer Cano,[8] Hallie C. Prescott,[1,8] Helen S. Goodridge,[9] and Rachel L. Zemans[1,10]

[1]Division of Pulmonary and Critical Care Medicine, Department of Internal Medicine, [2]Human Genetics, and [3]Computational Medicine and Bioinformatics, University of Michigan, Ann Arbor, Michigan, USA. [4]Department of Nephrology, University Hospital Regensburg, Regensburg, Germany. [5]Department of Microbiology and Immunology, [6]Department of Pathology, and [7]Gilbert S. Omenn Department of Computational Medicine and Bioinformatics, University of Michigan, Ann Arbor, Michigan, USA. [8]VA Center for Clinical Management Research, Ann Arbor, Michigan, USA. [9]Board of Governors Regenerative Medicine Institute and Department of Biomedical Sciences, Cedars-Sinai Medical Center, Los Angeles, California, USA. [10]Cellular and Molecular Biology Program, University of Michigan, Ann Arbor, Michigan, USA.

Patients who survive sepsis are predisposed to new hospitalizations for respiratory failure, but the underlying mechanisms are unknown. Using a murine model in which prior sepsis predisposes to enhanced lung injury, we previously discovered that classical monocytes persist in the lungs after long-term recovery from sepsis and exhibit enhanced cytokine expression after secondary challenge with intranasal LPS. Here, we hypothesized that immune reprogramming of post-sepsis monocytes and altered ontogeny predispose to enhanced lung injury. Monocyte depletion and/or adoptive transfer was performed 3 weeks and 3 months after sepsis. Monocytes from post-sepsis mice were necessary and sufficient for enhanced LPS-induced lung injury and promoted neutrophil degranulation. Prior sepsis enhanced JAK/STAT signaling and AP-1 accessibility in monocytes and shifted monocytes toward the neutrophil-like monocyte lineage. Neutrophil-like monocytes demonstrated a proinflammatory phenotype with enhanced IL-1β expression and reduced phagocytic capacity. In human sepsis and/or pneumonia survivors, monocytes were predictive of 90-day mortality and exhibited transcriptional and proteomic neutrophil-like signatures. We conclude that sepsis reprograms monocytes into a proinflammatory phenotype and skews bone marrow progenitors and monocytes toward the neutrophil-like lineage, predisposing them to induce neutrophil degranulation and lung injury.

Introduction

Nearly 40 million people survive sepsis each year (1), yet half of these survivors are rehospitalized or die within the following year (2–6). One in 20 sepsis survivors are rehospitalized with new lung injury, including conditions such as aspiration pneumonitis and exacerbation of chronic respiratory disease (2, 4). Our inability to develop effective strategies to prevent these complications stems from a limited understanding of the underlying mechanisms driving post-sepsis lung injury. Elevated inflammatory markers, such as circulating IL-6, C-reactive protein (CRP), and leukocyte counts, at hospital discharge have been associated with an increased risk of rehospitalization and mortality (7–10), suggesting that persistent immune dysregulation after sepsis may play a critical role (11).

To elucidate the mechanisms of lung injury in sepsis survivors, we previously developed a model of sterile lung injury in mice that have survived sepsis. In this model, cecal ligation and puncture (CLP) predisposes to enhanced lung injury in response to i.n. LPS administered 3 weeks after CLP (12). We discovered that monocytosis persists in the lungs for at least 3 weeks after sepsis alone, and these Ly6C^{hi} monocytes produced higher

Copyright: © 2026, Denstaedt et al. This is an open access article published under the terms of the Creative Commons Attribution 4.0 International License.

Submitted: August 1, 2025
Accepted: September 21, 2026
Published: September 24, 2026

Reference information: *JCI Insight*. 2026;11(21):e198551. https://doi.org/10.1172/jci.insight.198551.

levels of *Tnf* in response to i.n. LPS than monocytes in mice without prior sepsis (12). However, whether monocytes play a causal role in the enhanced lung injury induced by prior sepsis and the mechanisms through which sepsis might reprogram monocytes to exacerbate lung injury has not been studied.

Monocytes are known to play a direct role in regulating acute lung injury in the absence of prior sepsis. Ly6C^{hi} monocytes can either promote or mitigate lung injury depending on context (13–20). For instance, in *Klebsiella pneumoniae* infection, monocytes recruited to the lung are protective, whereas in influenza infection they are detrimental (14–19, 21). These observations suggest that monocytes assume diverse functional states and have led to a paradigm whereby the inflammatory milieu of the lung during injury dictates the activation status and function of recruited monocytes. This prevailing view relies on the assumption that circulating monocytes are a homogeneous population and also fails to consider how prior exposures may modulate recruitable monocyte functions or fates.

It is well established that infection can elicit durable reprogramming of immune cells and their progenitors in the BM, leading to enhanced (i.e., primed or trained) or suppressed (i.e., tolerant) responses to secondary stimuli (22–26). This reprogramming occurs via changes in transcriptional and epigenetic states, which may persist for weeks to months (24, 27–32). Such reprogramming typically involves activation or suppression of proinflammatory pathways. However, the ways in which cells are reprogrammed and the contexts in which immune reprogramming results in beneficial (e.g., host defense) or detrimental (e.g., tissue injury) responses to subsequent insults are vastly underexplored. Specifically, the extent to which respiratory complications in sepsis survivors are attributable to immune reprogramming, the specific cells that are reprogrammed, the mechanisms through which reprogrammed cells predispose to enhanced lung injury, and whether reprogramming may extend beyond alterations in inflammatory pathways are not known.

An emerging literature has revealed that BM Ly6C^{hi} monocytes comprise a heterogenous population of transcriptionally unique subsets (33–36), including those with distinct neutrophil-like and DC-like gene expression profiles, which are pre-determined during hematopoiesis. Critically, although single-cell RNA-Seq (scRNA-Seq) has characterized the transcriptomes of these monocyte subsets, aside from isolated studies (37–39), the specific functions of these subsets in homeostasis and disease remain unexplored. Specifically, the role of these monocyte subsets in acute lung injury and their contribution to the observed functional heterogeneity of monocytes in this context have not been investigated, to our knowledge. Moreover, whether immune reprogramming may involve not only the activation or suppression of proinflammatory pathways but also the reprogramming of mature monocytes and progenitors toward a particular lineage, thereby influencing responses to subsequent stimuli, has not been studied.

In this study, we address key questions regarding the functional heterogeneity and immune reprogramming of monocytes. We hypothesized that Ly6C^{hi} monocytes and/or their progenitors in the BM are reprogrammed by sepsis, thereby mediating enhanced post-sepsis lung injury. Through investigations of mouse models and human disease, we discovered that sepsis induces reprogramming of BM monocytes and their progenitors, leading to activation of proinflammatory pathways, altered hematopoiesis with a shift in progenitor cell fate toward the neutrophil-like monocyte lineage, and enhanced lung injury. Our findings introduce fundamental insights into the functions of potentially novel monocyte subsets and demonstrate that immune reprogramming can include not only changes in activation state but also shifts in ontogeny. Furthermore, by demonstrating that reprogramming of monocytes and their progenitors mediates the enhanced lung injury observed after sepsis, we challenge the paradigm that the lung milieu dictates functional monocyte responses during lung injury. Finally, we identify potentially novel therapeutic targets to reduce long-term pulmonary complications resulting in rehospitalization and mortality among sepsis survivors.

Results

Depletion of Ly6C^{hi} monocytes from post-CLP mice attenuates the lung injury response to LPS. We previously demonstrated that sepsis induced by CLP in mice induces persistent lung monocytosis at 3 weeks and, in response to subsequent i.n. LPS challenge, enhanced lung injury and *Tnf* expression by monocytes (12). However, whether monocytes play a functional role in this enhanced lung injury is unknown. We first confirmed an absence of alveolar-capillary barrier dysfunction, epithelial injury, or alveolar inflammation at 3 weeks after CLP (Supplemental Figure 1; supplemental material available online with this article; https://doi.org/10.1172/jci.insight.198551DS1). To determine whether Ly6C^{hi} monocytes are required for enhanced lung injury in 3-week post-CLP mice, we depleted monocytes using an anti-CCR2 antibody (αCCR2) administered prior to i.n. LPS (Figure 1A). Flow cytometric analysis of exudate

cells in bronchoalveolar lavage (BAL) confirmed effective depletion of monocytes and monocyte-derived exudate macrophages (Supplemental Figures 2 and 3). Post-CLP mice treated with αCCR2 antibody (post-$CLP_{αCCR2}$) had significantly reduced BAL albumin, indicating decreased lung permeability, at 72 hours after LPS relative to post-CLP mice treated with isotype control antibody (post-CLP_{ISO}) (Figure 1B). Importantly, in contrast to the protective effect of monocyte depletion on lung injury after CLP, monocyte depletion in unoperated control mice demonstrated a trend toward exacerbation of lung injury, as previously reported (14) (Figure 1C). Accordingly, there was less alveolar epithelial injury, as suggested by BAL receptor for advanced glycation end-product (RAGE) (40) levels in post-$CLP_{αCCR2}$ relative to post-CLP_{ISO} mice (Figure 1D). Neutrophil recruitment to the airspaces was unchanged (Figure 1E). Monocyte depletion significantly reduced BAL IL-6 levels (Figure 1F) but had little effect on other inflammatory mediators (Supplemental Figure 4). Taken together, these data demonstrate that monocytes mediate enhanced lung injury after LPS challenge in post-CLP mice.

Adoptive transfer of Ly6C^{hi} monocytes from post-CLP mice fails to protect against LPS-induced lung injury. Having shown that post-CLP monocytes are necessary for enhanced lung injury after LPS, we aimed to determine whether 3-week post-CLP monocytes are sufficient to exacerbate lung injury in response to LPS. Ly6C^{hi} monocytes from the BM of post-CLP or unoperated control mice were adoptively transferred into naive *Ccr2*$^{-/-}$ mice, followed by i.n. LPS administration (Figure 2A). The use of *Ccr2*$^{-/-}$ mice isolates the effect of the adoptively transferred *Ccr2*^{WT} monocytes, eliminating any potential confounding effects of endogenous recruited monocytes in the recipient mice. We confirmed that transferred monocytes entered the lung and airspace, home to the lung, and displayed features of macrophage differentiation after transfer (Supplemental Figure 5). Consistent with prior literature (14) and our monocyte depletion experiments (Figure 1), transfer of *Ccr2*^{WT} monocytes harvested from unoperated control mice tended to decrease lung permeability, as measured by BAL albumin, compared with transfer of *Ccr2*$^{-/-}$ monocytes (Figure 2B). In contrast, post-CLP monocyte transfer resulted in increased BAL albumin and total protein relative to *Ccr2*^{WT} unoperated control monocytes (Figure 2, B and C). There were no differences in neutrophil recruitment to the airspace (Figure 2D) or in levels of most cytokines and chemokines (Figure 2E and Supplemental Figure 6). Collectively, Figures 1 and 2 show that post-CLP Ly6C^{hi} monocytes are detrimental in LPS-induced lung injury in contrast to the more protective functional program of unoperated control Ly6C^{hi} monocytes, suggesting that CLP reprograms monocytes from a protective phenotype to an injurious phenotype.

Post-CLP Ly6C^{hi} monocytes promote neutrophil activation and degranulation in response to LPS. Lung permeability in LPS-induced lung injury is neutrophil dependent (41–45). However, despite alterations in lung permeability, we observed no differences in neutrophil recruitment after monocyte depletion and adoptive transfer (Figure 1E and Figure 2D), suggesting that the mechanism by which post-CLP monocytes enhance lung injury is not via augmented neutrophil recruitment. Therefore, we hypothesized that post-CLP monocytes may enhance neutrophil activation. We previously observed elevated levels of S100A8/A9, a damage associated-molecular pattern protein released upon neutrophil activation (46–49), in the BAL of post-CLP mice after i.n. LPS (12). Here, we found that in post-CLP mice, adoptive transfer of post-CLP monocytes increased BAL S100A8/A9 (Figure 3A), whereas monocyte depletion reduced BAL S100A8/A9 (Figure 3B), suggesting that post-CLP monocytes activate neutrophils.

A key facet of neutrophil activation is degranulation, the release of granule contents — such as proteolytic enzymes, antimicrobial peptides, and other substances that contribute to lung injury (49–52) — into the extracellular space. To investigate whether post-CLP monocytes directly induce neutrophil activation and degranulation, we isolated BM Ly6C^{hi} monocytes from post-CLP mice stimulated with LPS, transferred the monocyte conditioned media (CM) to naive BM neutrophils, and measured markers of neutrophil activation/degranulation (Figure 3C). Prior to transfer, we confirmed that monocyte CM from post-CLP and control mice did not differ in these products (Figure 3D and Supplemental Figure 7). The CM from post-CLP monocytes induced greater release of S100A8/A9 (Figure 3D) and the neutrophil granule proteins myeloperoxidase (MPO), neutrophil gelatinase-associated lipocalin (NGAL), and matrix metallopeptidase 9 (MMP9) than CM from unoperated control monocytes (Figure 3E). These data suggest that post-CLP monocytes enhance neutrophil activation and degranulation, thereby contributing to enhanced lung injury.

Enhanced lung injury in post-CLP mice persists for 3 months. Prior infection or inflammation can have durable effects on subsequent inflammatory responses (22–26). Therefore, we hypothesized that the enhanced lung injury response observed in sepsis survivor mice may be durable far beyond 3 weeks after CLP. We therefore evaluated the lung injury response at 3 months after CLP (Figure 4A). We again confirmed that CLP did not

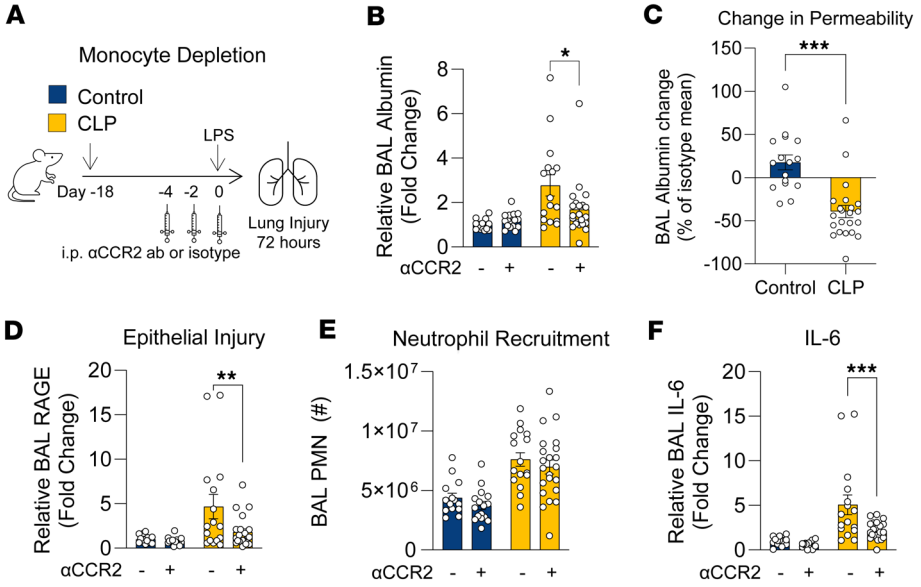


Figure 1. Monocyte depletion improves lung injury and inflammation in post-CLP mice. (**A**) Experimental design for monocyte depletion with anti-CCR2 antibody (αCCR2) or isotype prior to i.n. LPS. (**B**–**F**) Lung permeability assessed by BAL albumin (**B**), change in permeability relative to isotype treatment for each condition (**C**), epithelial injury assessed by BAL RAGE (**D**), neutrophil recruitment (**E**), and BAL IL-6 (**F**) shown 72 hours after i.n. LPS. *n* = 4–8 per group, 3 cohorts; 2 of 18 mice in the iso-treated CLP group died by 72 hours; no other deaths were recorded. BAL protein levels expressed relative to the mean of isotype-treated unoperated control mice. Mean ± SEM, Šidák's post hoc *P* value (**B** and **D**–**F**), Welch's *t* test (**C**) shown. **P* < 0.05, ***P* < 0.01, ****P* < 0.001. PMN, polymorphonuclear.

induce persistent alveolar-capillary barrier permeability, epithelial injury, or alveolar inflammation (Supplemental Figure 8). Remarkably, post-CLP mice exhibited significantly increased lung permeability and epithelial injury compared with control mice (Figure 4, B and C). This was accompanied by increased airspace neutrophils and IL-6 levels (Figure 4, D and E). Adoptive transfer of monocytes from 3-month post-CLP mice resulted in increased lung permeability relative to transfer of unoperated control monocytes (Figure 4F). These findings confirm that enhanced lung injury after recovery from sepsis is a durable phenotype that is mediated by monocytes. This durable proinflammatory phenotype is consistent with reprogramming of monocytes, wherein monocytes are primed for enhanced responses to a secondary stimulus.

CLP elicits proinflammatory transcriptional and epigenetic reprogramming of Ly6C^{hi} monocytes. The enhanced lung injury and neutrophil activation mediated by monocytes after sepsis, particularly in contrast to the protective role of monocytes in lung injury without preceding sepsis, imply that sepsis reprograms Ly6C^{hi} monocytes toward a primed state that promotes a more robust proinflammatory response to secondary stimuli. Such immune reprogramming after an initial stimulus is typically attributable to transcriptional and epigenetic alterations (23). We hypothesized that CLP induces persistent alterations in the transcriptome and/or epigenome of monocytes. To investigate these alterations, we performed bulk RNA-Seq and ATAC-Seq on mature BM Ly6C^{hi} monocytes isolated at 3 weeks after CLP (Supplemental Figure 9). We found CLP was associated with significant upregulation of 181 genes and downregulation of 181 genes consistently across samples (Figure 5A). Pathway analysis of gene expression data revealed that post-CLP monocytes were enriched for pathways related to HIF-1α, cell cycle, glucose/lipid metabolism, and inflammatory signaling relative to the control (Figure 5B). Specifically, post-CLP monocytes upregulated TLR (*Tlr4*, *Lbp*, *Myd88*, *Mapk13*) and JAK/STAT pathway genes while downregulating other antiinflammatory genes (*Nfkbia*, *Nfkbie*, *Igf1*) (Supplemental Figure 10A). ATAC-Seq identified enrichment of uniquely accessible promoter and enhancer regions, indicating active or poised transcription, in post-CLP monocytes. Accessible promoters were linked to genes in glycolytic and inflammatory pathways (Figure 5C). The JAK/STAT signaling pathway was enriched in both the promoter (Figure 5C) and enhancer (Figure 5D) regions in post-CLP monocytes. In contrast, promoter regions in monocytes from unoperated control mice were enriched for homeostatic pathways, including vesicle transport, fatty acid biosynthesis/signaling, acetyl-CoA handling, and nucleotide metabolism (Supplemental Figure 10B). To identify the transcription factors that potentially bind these open genomic regions, we conducted motif enrichment analysis (53). This analysis identified Fos/Jun motifs for the dimeric activator protein-1 (AP-1) transcription factors in enhancer

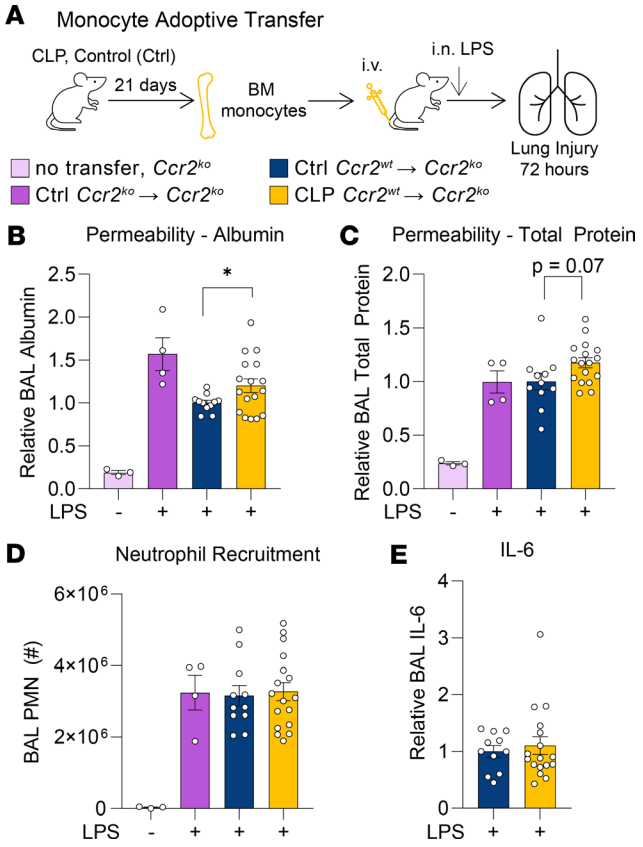


Figure 2. Adoptive transfer of post-CLP monocytes enhances the lung injury response to LPS. (**A**) BM Ly6C^{hi} monocytes from *Ccr2*$^{-/-}$, *Ccr2*^{WT} age-matched unoperated control, and *Ccr2*^{WT} 3-week post-CLP mice were isolated and i.v. administered to *Ccr2*$^{-/-}$ mice concurrently with i.n. LPS. (**B**–**E**) Alveolar permeability assessed by BAL albumin or total protein (**B** and **C**), neutrophil recruitment (**D**), and BAL IL-6 (**E**) shown 72 hours after i.n. LPS. BAL protein measurements expressed relative to the mean of unoperated control *Ccr2*^{WT} transfer for each cohort. *n* = 3–6 per group, 3 cohorts. Mean ± SEM, Welch's *t* test *P* value shown. **P* < 0.05, ***P* < 0.01. PMN, polymorphonuclear.

regions of post-CLP monocytes (Figure 5E), including a nearly 3-fold increase in the number of genes with at least one enhancer peak containing the AP-1 motif (Figure 5F). In other inflammatory contexts, AP-1 binding to enhancer regions of DNA is essential for maintaining chromatin accessibility and the enhanced inflammatory mediator production in response to secondary challenge that characterizes a durable form of reprogramming known as immune memory (54–56). Together, these data demonstrate transcriptional and epigenetic reprogramming of BM Ly6C^{hi} monocytes toward a persistently primed state.

Sepsis induced by CLP reprograms monocytes toward the neutrophil-like lineage. Recent scRNA-Seq studies have begun to uncover subsets of classical monocytes (33–36, 57, 58). These studies identify 2 trajectories through BM progenitors whereby monocyte progeny express typical genes for neutrophils and DCs, neutrophil-like and DC-like monocytes, respectively (Figure 6A). Deeper interrogation of our multiomics data revealed that post-CLP monocytes upregulated neutrophil-specific genes (e.g., neutrophil granule protein *Ngp*, proteinase-3 *Prtn3*, lipocalin-2 *Lcn2*), while downregulating DC-specific genes (e.g., *Cd209a*) (Figure 6B). Although the transcriptomes of these subsets have been characterized by scRNA-Seq, to our knowledge, aside from isolated studies (38, 59), the specific functions of these novel monocyte subsets remain unexplored. Moreover, to our knowledge, these monocyte subsets have not been characterized in the context of prior sepsis and lung injury. Based on the increased expression of neutrophil-like monocyte genes in post-CLP monocytes (Figure 6B), we hypothesized that CLP reprograms monocytes toward a neutrophil-like state. To confirm this, we conducted gene signature enrichment analysis using gene modules specific to neutrophil-like and DC-like monocytes (33). Monocytes from post-CLP mice were enriched for the neutrophil-like (granulocyte-monocyte progenitor [GMP] derived) monocyte signature, while control monocytes were enriched for the DC-like (monocyte-DC progenitor [MDP] derived) monocyte signature, suggesting that CLP induces expansion of the neutrophil-like monocyte population (Figure 6C).

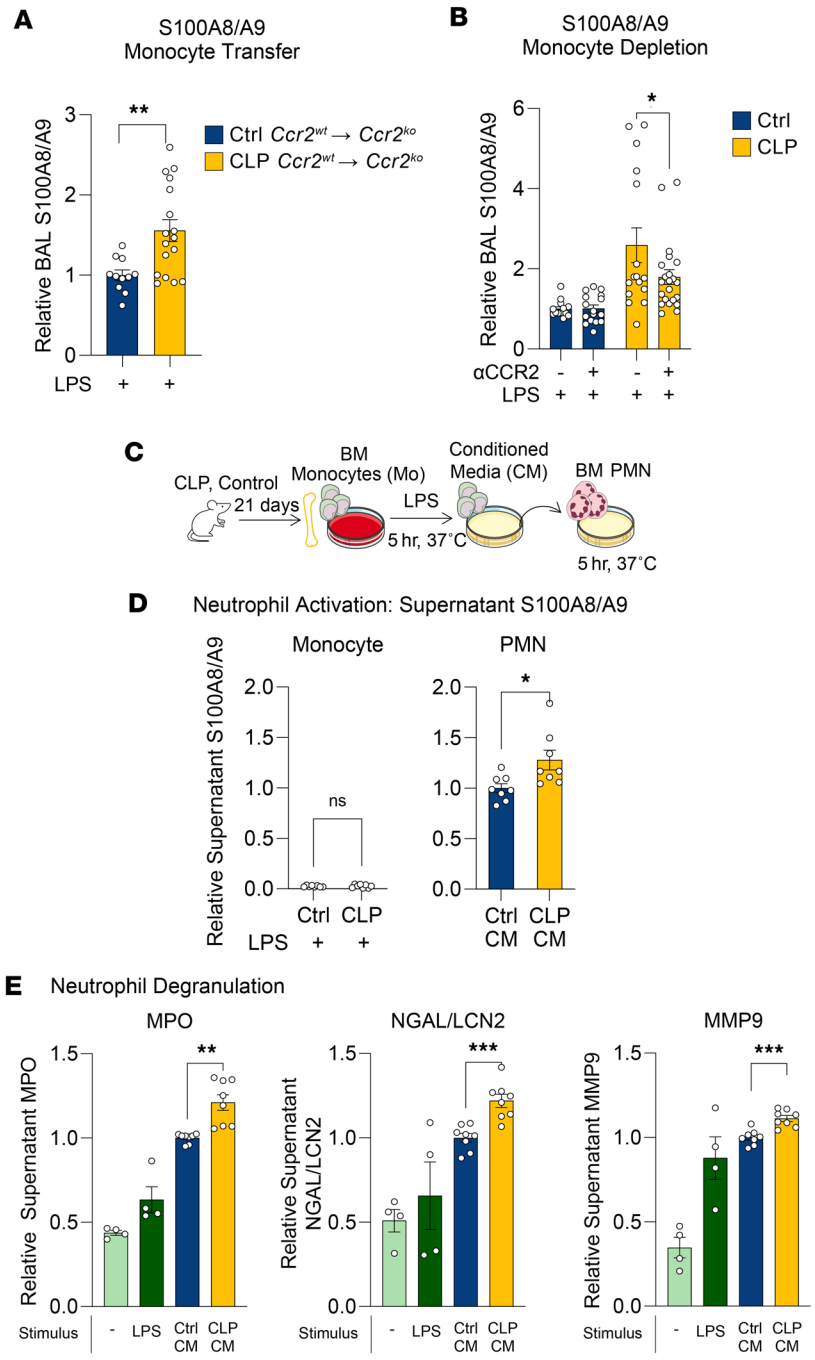


Figure 3. Post-CLP monocytes promote activation and degranulation of neutrophils. (**A** and **B**) BAL S100A8/A9 after adoptive transfer (**A**) and antibody-mediated depletion of BM Ly6C^{hi} monocytes (**B**) measured 72 hours after i.n. LPS. (**C** and **D**) Monocyte and neutrophil S100A8/A9 production in supernatants after stimulation with LPS or monocyte CM, respectively. (**E**) Neutrophil granule proteins were measured to assess degranulation induced by monocyte CM. n = 4 mice per group, 2 cohorts. Supernatant protein expressed relative to the mean of unoperated control monocyte CM. Mean ± SEM, Welch's t test P value shown. *P < 0.05, **P < 0.01, ***P < 0.01. PMN, polymorphonuclear.

To confirm expansion of the neutrophil-like monocyte population after CLP, we first analyzed forward-scatter (FSC) and side-scatter (SSC) flow cytometric properties of Ly6C^{hi} monocytes, as larger size and increased granularity have been shown to identify neutrophil-like monocytes (33). We identified 2 populations of monocytes within the Ly6C^{hi} fraction: FSC^{lo}SSC^{lo} and FSC^{hi}SSC^{hi}. Post-CLP mice exhibited a 2- to 3-fold increase in FSC^{hi}SSC^{hi} Ly6C^{hi} cells, consistent with neutrophil-like monocyte expansion (Figure 6D). To further validate expansion of neutrophil-like monocytes after CLP, we used

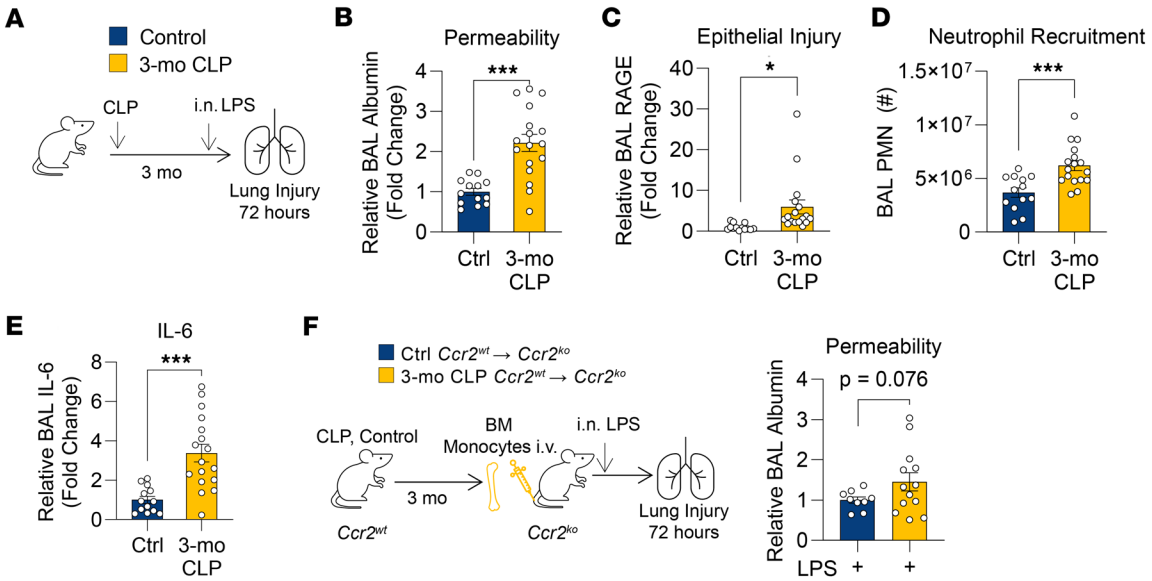
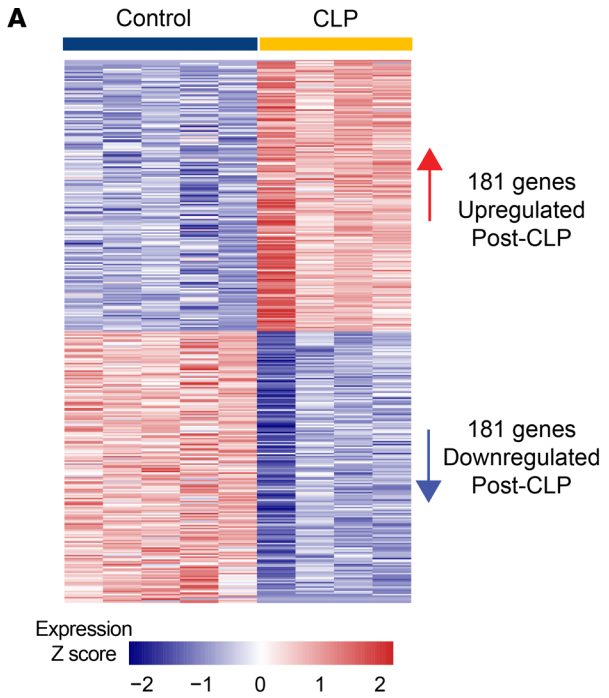


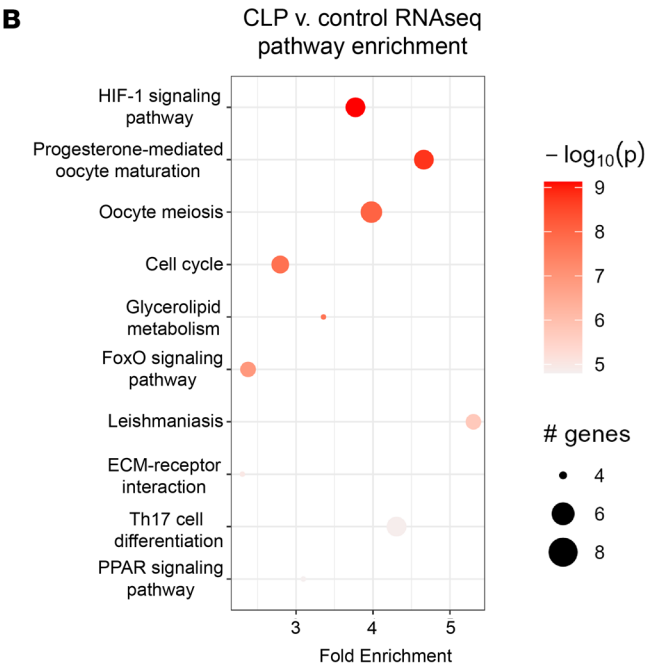
Figure 4. Monocyte-mediated enhanced lung injury in post-CLP mice is durable. (**A**) Three-month post-CLP and age-matched control mice were administered i.n. LPS. (**B**–**E**) Alveolar permeability assessed by BAL albumin (**B**), epithelial injury assessed by BAL RAGE (**C**), neutrophil recruitment (**D**), and BAL IL-6 (**E**) measured 72 hours after i.n. LPS. (**F**) BM Ly6C^{hi} monocytes were isolated from *Ccr2*^{WT} age-matched unoperated control and *Ccr2*^{WT} 3-month post-CLP mice and i.v. administered to *Ccr2*$^{-/-}$ mice concurrently with i.n. LPS; alveolar permeability was assessed by BAL albumin. n = 5–10 per group, 2 cohorts (**A**–**E**), n = 2–6 per group, 3 cohorts (**F**). Mean ± SEM, Welch's t test P value shown. *P < 0.05, **P < 0.01, ***P < 0.001. PMN, polymorphonuclear.

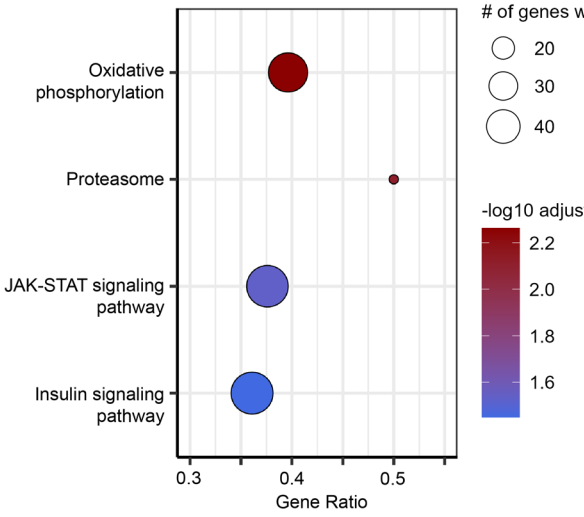
Gfi1-tdTomato mice, which identify this lineage due to their higher levels of *Gfi1* (33) (Supplemental Figure 11A). We observed higher *Gfi1* expression in the Ly6C^{hi} monocytes (Figure 6E). In fact, tomato fluorescence in the FSC^{hi} population was comparable to neutrophils and significantly greater than FSC^{lo} monocytes, strongly suggesting that the Gfi1^{hi} cells represent neutrophil-like monocytes. To confirm that sepsis induces expansion of neutrophil-like monocytes, we performed CLP on *Gfi1*-tdTomato mice and found that Gfi1^{hi}FSC^{hi} monocytes were significantly increased in post-CLP mice (Figure 6F). These data confirm that CLP reprograms monocytes toward the neutrophil-like lineage.

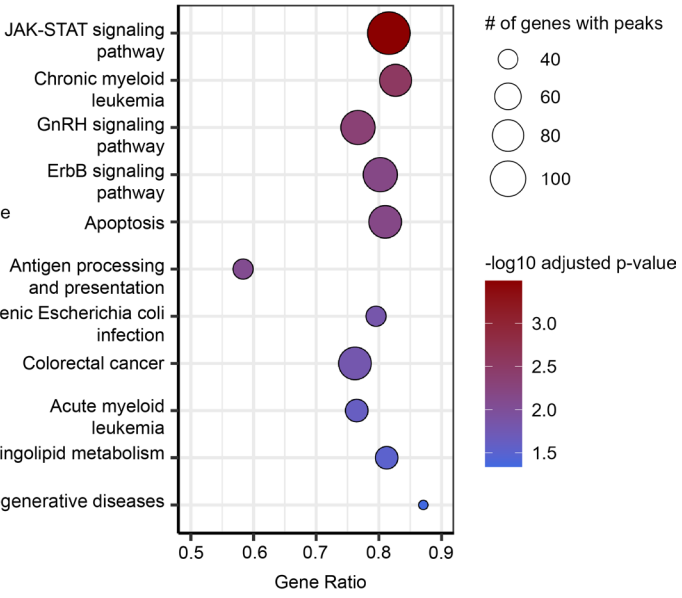
Recent work has identified monocytes with neutrophil-like features derived from the GMP in other contexts (34, 39, 57), identifying both increased phagocytosis and myeloid suppressor functions in GMP-lineage monocytes. To determine the relationship of our Gfi1^{pos} monocytes with those previously reported, we identified 2 populations, Gfi1^{pos} and Gfi1^{neg}, within the GMP lineage (Supplemental Figure 11A). To determine the functions of Gfi1^{pos} monocytes and their potential role in post-CLP enhanced lung injury, we evaluated the secretory response to LPS, phagocytosis, and efferocytosis. We found that Gfi1^{pos} monocytes secreted 4–5 times more IL-1β and similar IL-1ra relative to Gfi1^{neg} monocytes, suggesting a proinflammatory phenotype (Figure 6G). We also found that Gfi1^{pos} monocytes were significantly less phagocytic (Figure 6H) and tended to be less efferocytic (Supplemental Figure 11B). Prior work has suggested that monocytes with neutrophil-like gene expression are immunoregulatory (34), displaying features of myeloid derived suppressor cells (MDSCs). We found that post-CLP monocytes were variably enriched for MDSC genes, indicating a potential MDSC-like phenotype (Supplemental Figure 11C). Finally, we evaluated whether post-CLP monocytes in the BM are similar to those recently described in scRNA-Seq of the spleen after CLP (57). We found that our BM post-CLP monocytes upregulated similar genes to the neutrophil-like monocyte substates recently described in the spleen (Supplemental Figure 11D). Together, these data suggest that Gfi1^{pos} neutrophil-like monocytes display a proinflammatory and MDSC-like profile, suggesting a potential role in enhanced lung injury phenotypes.

CLP reprograms BM monocyte progenitors toward the neutrophil-like lineage. Given that sepsis leads to a durable expansion of the neutrophil-like monocyte population, but the half-life of monocytes is only hours to days (58, 60), we hypothesized that sepsis survival shifts hematopoiesis and monocyte fate toward the neutrophil-like lineage at the level of monocyte progenitors. Previous studies using ex vivo culture of monocyte progenitors revealed that neutrophil-like monocytes arise from the GMP via their own monocyte-committed progenitor (MP), while DC-like monocytes arise from the MDP via the common monocyte progenitor (cMoP) (Figure 6A).









E CLP v. control TF known motif enrichment

Rank	Consensus Sequence	Motif	Q-value
1		FOS	9.11e-08
2		FOS::JUND	9.11e-08
3		FOS::JUNB	1.71e-07
4		FOSL2::JUN	1.89e-07
5		FOSB::JUNB	2.47e-07

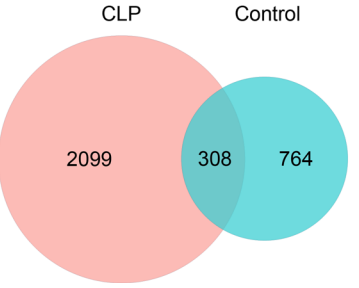


Figure 5. Transcriptional and epigenetic pathways contributing to post-CLP monocyte priming. (**A**) Ly6C^{hi} monocytes were isolated from BM for transcriptomic and epigenomic profiling. Heatmap of differentially expressed genes in post-CLP mice compared with unoperated control mice. (**B**) Top 10 transcriptomic pathways enriched in 3-week post-CLP monocytes relative to control. (**C** and **D**) In a separate experiment, ATAC-Seq was performed, unique peaks were identified, and pathway enrichment performed on promoter (**C**) and enhancer regions (**D**). (**E**) Known motif enrichment performed relative to control monocytes' genomic background. (**F**) Quantification of shared and differentially expressed peaks containing the AP-1 binding motif in post-CLP and control monocytes. n = 4–5 mice per group. TSS, transcription start site.

To specifically assess expansion of the GMP-derived lineage in the BM, we flow-sorted the MP plus cMoP fraction (Supplemental Figure 12), performed bulk RNA-Seq, and assessed for enrichment of MP and cMoP progenitor gene signatures. Consistent with our hypothesis, post-CLP BM progenitors were enriched for the MP signature (Figure 7A). We then directly assessed for GMP expansion in the BM of post-CLP mice, using established surface markers of GMPs (61). We demonstrated an increase in GMP progenitors in post-CLP mice compared with controls, without changes in MDP (Figure 7B). Consistent with expanded GMP, which produce neutrophils as well as monocytes, we found a concomitant increase in WBCs characterized by increased circulating neutrophils and monocytes in post-CLP mice (Figure 7C). Persistent expansion of GMP and their downstream progeny is highly suggestive of recent or ongoing myelopoiesis, which can be driven by CSFs. We found that this BM phenotype 3 weeks after CLP was associated with persistent low-grade elevations in circulating granulocyte-CSF (G-CSF) (Figure 7D).

In summary, these data suggest that sepsis induced by CLP reprograms hematopoietic progenitors, resulting in a shift in monocyte ontogeny toward the GMP lineage, thereby expanding neutrophil-like monocytes and their progenitors, MPs and GMPs. Coupled with the demonstrated functional role of post-CLP monocytes in exacerbating LPS-induced lung injury (Figures 1 and 2), these data suggest that a shift in BM ontogeny toward the neutrophil-like monocyte subset promotes enhanced lung injury in post-CLP mice. These data also suggest that GMP-lineage skewing and co-mobilization of monocytes and neutrophils in circulation in post-CLP mice may be driven by ongoing production of CSFs (e.g., G-CSF).

Neutrophil-like monocytes are expanded by acute human sepsis, and monocyte counts predict long-term mortality in human sepsis survivors. Patients who survive sepsis are at increased risk of long-term rehospitalization and death (2, 3), yet the underlying mechanisms remain unclear. Given the role of monocytes in mediating enhanced acute lung injury in sepsis survivor mice (Figures 1 and 2), we hypothesized that mobilization of monocytes may similarly predict poor long-term outcomes after sepsis in humans. We previously demonstrated that abnormal leukocyte counts at the time of hospital discharge predict 90-day rehospitalization and/or death (9) in patients surviving sepsis; here, we examined whether absolute monocyte count (AMC) at hospital discharge would also predict 90-day mortality. Using a United States Veterans Affairs (VA) health system dataset (62), we identified 92,165 patients who met inclusion criteria for sepsis (Supplemental Figure 13), 13.6% of whom died within 90 days (Supplemental Table 1), consistent with our prior findings (9). We found that AMC was associated with an increased hazard ratio for 90-day mortality (Figure 8A).

We next investigated whether the monocytes associated with mortality in patients with sepsis could be enriched for neutrophil-like features. In our murine sepsis model, concurrent expansion of neutrophils and monocytes (Figure 7C) reflected mobilization of the GMP lineage and persistent G-CSF signaling. We have shown independently that AMC (Figure 8A) and absolute neutrophil count (ANC) were associated with 90-day mortality (9). To gain insight into whether the associations between increased AMC and mortality and increased ANC and mortality may indicate mobilization of a common progenitor linked to poor outcomes, we first analyzed whether the predictive value of monocyte count was dependent on neutrophil count by plotting the hazard ratio surface for the interaction of AMC and ANC for 90-day mortality (Figure 8B). The hazard ratio for AMC increased most markedly as ANC increased. This indicates that the prognostic value of AMC is highly dependent on the concomitant ANC, suggesting that AMCs are most predictive of poor outcome when the common progenitor is mobilized. Since monocytes and neutrophils both derive from GMPs, our findings suggest persistent mobilization of the GMP lineage is highly associated with poor outcomes in patients with sepsis.

To acquire further evidence to establish whether neutrophil-like monocytes were expanded in acute human sepsis, we interrogated publicly available RNA-Seq datasets of bulk human CD14^{+} monocytes from patients with sepsis for evidence of a neutrophil-like gene signature (63–66). To assess enrichment of monocyte subsets, we utilized neutrophil-like and DC-like monocyte gene signatures conserved between mice and humans (67). As expected, these signatures detected the enrichment of GMP-derived neutrophil-like monocytes in our CLP mouse model of sepsis (Supplemental Figure 14). We then assessed the

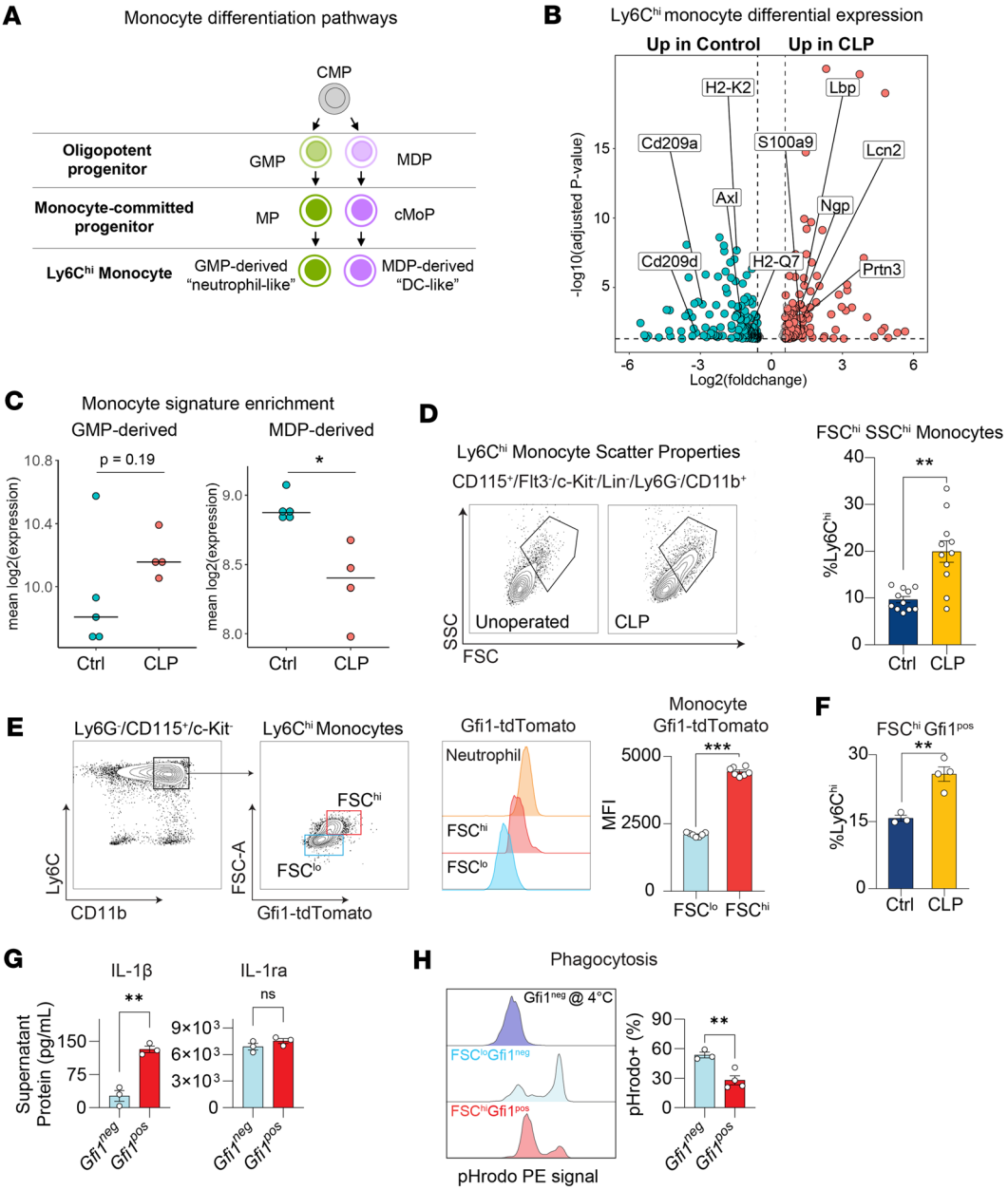


Figure 6. Neutrophil-like monocytes are expanded in post-CLP mice prior to LPS administration. (**A**) Monocyte differentiation pathways (33). (**B**) Differential gene expression in BM Ly6C^{hi} monocytes without LPS exposure highlighting neutrophil- and DC-specific genes. (**C**) Enrichment of GMP-derived and MDP-derived monocyte signatures (33) in Ly6C^{hi} monocytes. (**D**) Scatter properties of Ly6C^{hi} monocytes in post-CLP and unoperated control mice. (**E**) Gfi1-tdTomato fluorescent intensity in neutrophils and FSC^{hi} or FSC^{lo} monocytes. Proportions of FSC^{hi}Gfi1-tdTomato Ly6C^{hi} monocytes in post-CLP and unoperated control mice (**F**). (**G** and **H**) Gfi1^{pos} and Gfi1^{neg} IL-1β and IL-1ra secretion in response to LPS (**G**) and phagocytosis of pHrodo *E. coli* particles (**H**). n = 4–5 per group, 2 cohorts (**D**), n = 3–5 mice per group, 1 cohort (**B**, **C**, **E**, and **F**), n = 1–2, 2 cohorts (**G** and **H**). Mean, Wilcoxon's rank-sum test (**C**); mean ± SEM and Welch's t test (**D**–**H**) are shown. *P < 0.05, **P < 0.01.

expression of individual neutrophil-like and DC-like genes by CD14$^+$ monocytes using bulk RNA-Seq data from multiple distinct cohorts of patients with sepsis or pneumonia (64, 65). We observed upregulation of conserved neutrophil-like genes (*S100A9*, *IL1R2*, *LRG1*) and downregulation of genes associated with DCs (*CD74*, *HLA-DMA*, *HLA-DRB5*) (Figure 8, C and D). To validate the expansion of neutrophil-like monocytes in patients, we next examined the proteome of CD14$^+$ monocytes in patients with bacterial sepsis (66) (Figure 8E). We again found enrichment of neutrophil-like proteins in the monocytes of patients with sepsis. This consistent observation of increased levels of neutrophil genes and proteins across multiple independent cohorts of acute pneumonia and sepsis suggests a shift toward a neutrophil-like state in acute infectious/inflammatory human disease of diverse etiologies.

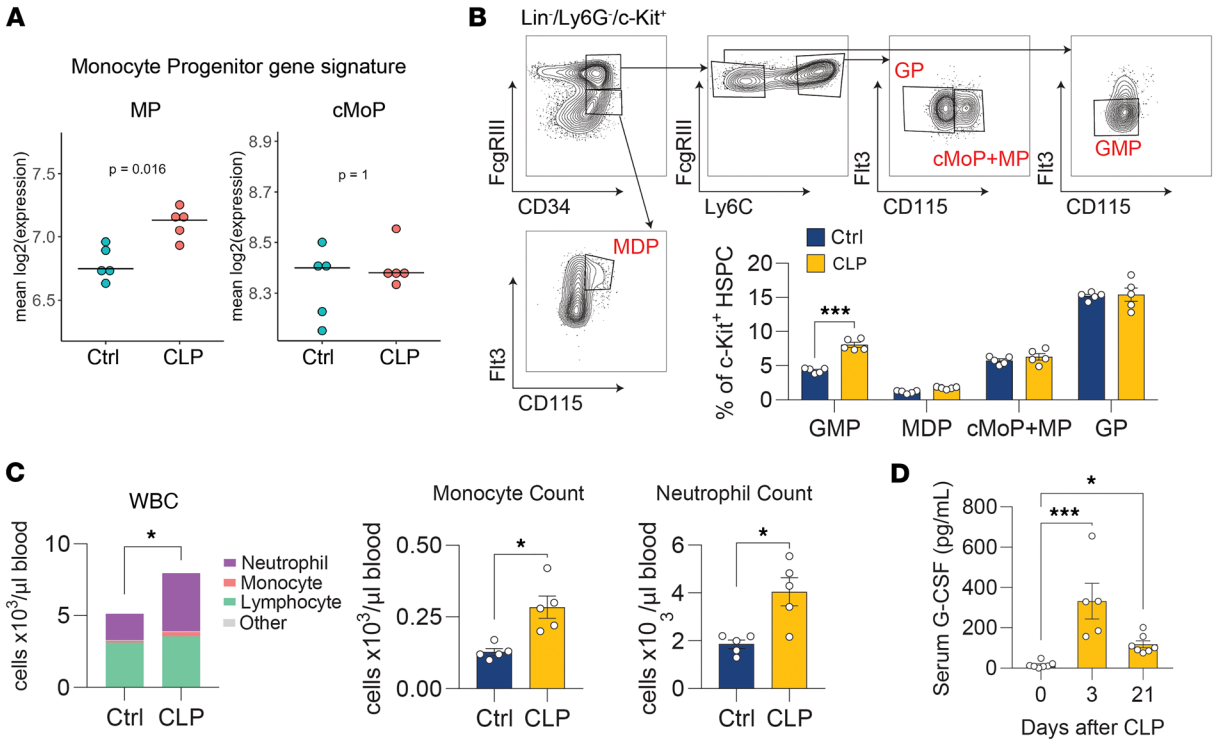


Figure 7. CLP alone reprograms progenitors toward GMP lineage. (**A**) Monocyte-committed BM progenitors (MP + cMoP enriched) were isolated from BM from 3-week post-CLP and unoperated control mice prior to LPS administration and tested for enrichment of MP (GMP-derived) and cMoP (MDP-derived) signatures (33). (**B**) Quantification of myeloid progenitors by flow cytometry. (**C** and **D**) Peripheral blood counts (**C**) and serum G-CSF levels (**D**) in 3-week post-CLP mice and unoperated controls prior to LPS administration. n = 4–5 per group, 1 cohort (**A**–**C**), n = 2–5, 2 cohorts (**D**). Mean, Wilcoxon's rank-sum test (**A**); mean ± SEM and Welch's t test (**B** and **C**) are shown. $^*P < 0.05$, $^{**}P < 0.01$, $^{***}P < 0.01$.

Finally, to confirm that enrichment of the neutrophil-like signature in bulk CD14$^+$ monocytes reflects expansion of a neutrophil-like population in acute sepsis, we explored an scRNA-Seq dataset of CD14$^+$ monocytes from patients with acute bacterial infection and sepsis (63). Unbiased clustering previously revealed 4 monocyte states (MS1–MS4) (63), and the MS1 cluster was expanded in patients with bacterial infection and sepsis. To determine whether MS1 represents a neutrophil-like monocyte, we examined the conserved monocyte subset gene signatures across the 4 monocyte states. Consistent with our hypothesis, the MS1 cluster consistently upregulated neutrophil-like genes and downregulated DC-like genes, suggesting that MS1 is indeed a neutrophil-like state (Figure 8F). Thus, the alterations observed in bulk monocytes from patients with sepsis (Figure 8, C–F) likely reflect expansion of neutrophil-like monocytes. Taken together, these data strongly suggest that neutrophil-like monocytes are mobilized in both mice and humans with sepsis and may promote poor outcomes.

Discussion

As survival rates for sepsis improve, more patients are at risk of post-sepsis complications, including rehospitalization with new organ injury. Herein, we demonstrated that sepsis induced by CLP in mice durably reprograms Ly6C^{hi} monocytes, predisposing to enhanced lung injury upon LPS challenge. We identified key transcriptomic and epigenomic signatures persistently activated after CLP, including JAK/STAT and AP-1. Moreover, CLP induces Ly6C^{hi} monocytes and their progenitors to shift toward the GMP-derived neutrophil-like lineage in association with persistent G-CSF signaling. Functionally, we find that neutrophil-like monocytes display proinflammatory features, including significantly enhanced IL-1β production, which could promote lung injury. Monocytes reprogrammed by sepsis also promote neutrophil activation. Importantly, we discovered that monocyte counts predict long-term outcomes in human sepsis survivors and that monocytes are similarly enriched for a neutrophil-like signature during acute sepsis. These data support a conceptual model whereby sepsis reprograms the immune activation state and ontogeny of monocytes and their progenitors, leading to a sustained risk for new organ injury.

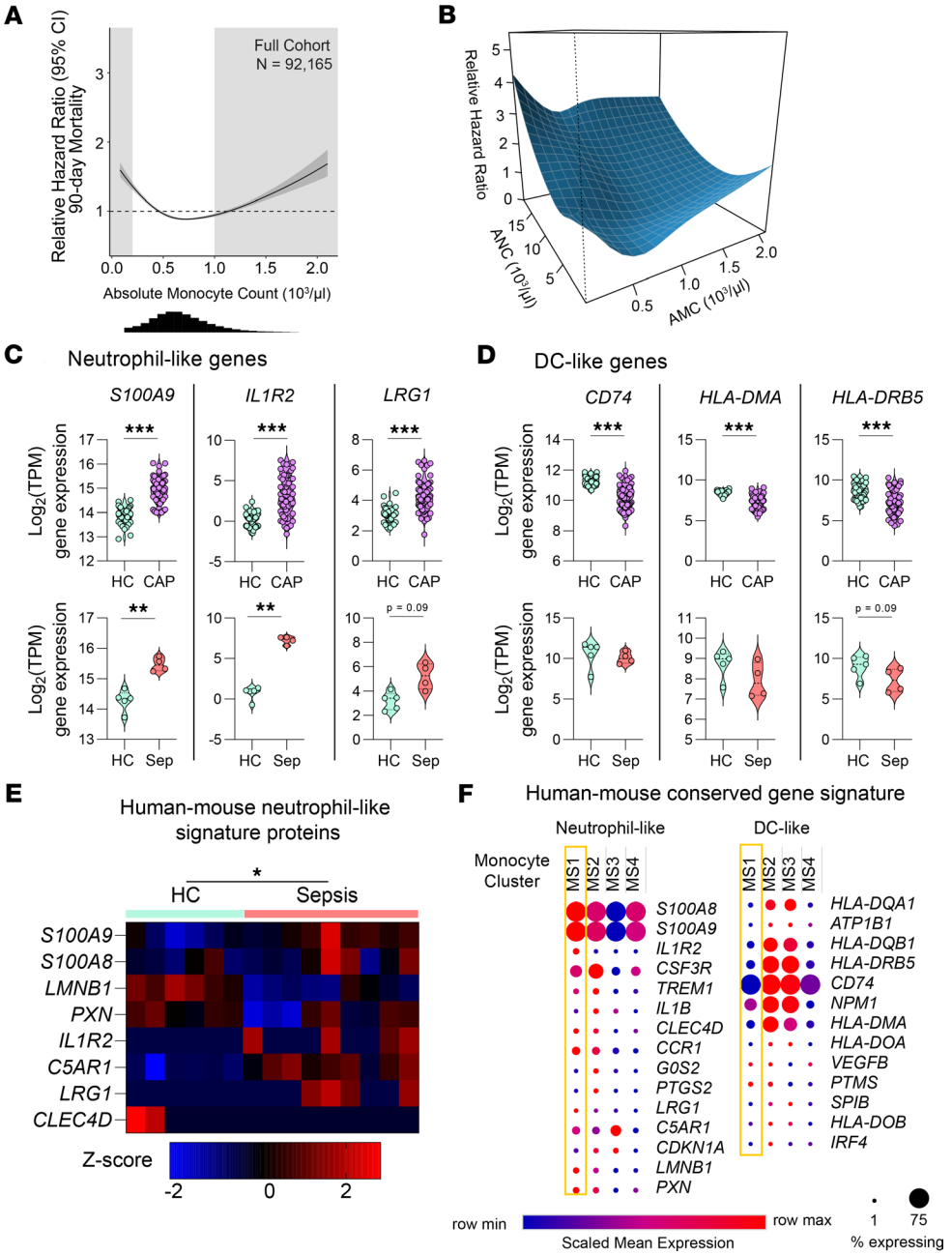


Figure 8. Neutrophil-like monocytes in patients with sepsis. (**A**) Unadjusted Cox proportional hazard regression (95% CI, dark gray) with relative hazard ratio for 90-day mortality for absolute monocyte count (AMC); histogram of AMC distribution shown below. (**B**) Light gray boxes indicate values outside of the normal clinical range; 3D interaction surface showing the relationship of AMC and ANC with 90-day mortality. (**C** and **D**) Selected neutrophil-like and DC-like gene expression in CD14$^+$ monocytes in patients with acute sepsis (n = 4 sepsis, 5 healthy) (64) and community acquired pneumonia (CAP n = 69; 41 healthy) (65). (**E**) Conserved human-mouse (67) neutrophil-like signature proteins in classical monocytes from patients with sepsis (66). Proteins detected in more than 1 sample across conditions were included in the heatmap, and missing values were imputed as described in the Methods. (**F**) Conserved human-mouse neutrophil-like and DC-like signature genes across monocyte substates (MS1–4) in scRNA-Seq performed in patients with acute bacterial infection (63). Mean, 25th and 75th percentile, Welch's t test shown (**C** and **D**). Multivariate-ANOVA P value shown (**E**). *P < 0.05, **P < 0.01, ***P < 0.001. HC, healthy control. Sep, sepsis.

These findings significantly advance our understanding of functional monocyte heterogeneity. Although an emerging literature has revealed that Ly6C^{hi} monocytes are heterogenous (33–36), the specific contexts in which monocyte subsets arise and their functional roles in disease pathogenesis remain significant and clinically relevant gaps in our knowledge (68, 69). Neutrophil-like and DC-like subsets of

Ly6C^{hi} monocytes have recently been identified by scRNA-Seq in both homeostasis and sterile inflammation in multiple species (33–36, 39). Here, we demonstrate that neutrophil-like monocytes expand in murine and human sepsis**.** Using the CLP mouse model, we demonstrate expansion of neutrophil-like monocytes via multiple methods: gene expression analysis, flow cytometric (FSC/SSC) characteristics, and the use of a Gfi1-reporter mouse (Figures 6 and 7). We also find that our GMP-lineage/Gfi1^{pos} neutrophil-like monocytes are transcriptionally similar to those identified in the spleen after CLP using scRNA-Seq (Supplemental Figure 11) (57), indicating expansion of neutrophil-like monocytes across sites of hematopoiesis after sepsis. Importantly, we also confirm the expansion of neutrophil-like monocytes in humans with sepsis as well as pneumonia (Figure 8), demonstrating that this phenomenon is conserved across species and across multiple acute infectious/inflammatory human diseases.

However, the greatest impact of this work lies in the functional studies. Our data strongly suggest that the durable expansion of the neutrophil-like monocytes induced by sepsis (Figure 6) exacerbates subsequent lung injury in mice (Figures 1, 2, and 4). We further demonstrate that Gfi1^{pos} neutrophil-like monocytes are proinflammatory, secreting 4–5 times more IL-1β. We also show reduced phagocytic and efferocytic capacity in GMP-lineage Gfi1^{pos} monocytes relative to Gfi1^{neg}, which diverges from recent reports of increased phagocytosis in CD177^{+} GMP-lineage monocytes and post-CLP monocytes reported by others (34, 57), suggesting functional heterogeneity within the GMP lineage. Following isolated reports (38, 39, 59), our study represents one of the first demonstrations of specific functions of neutrophil-like monocytes, to our knowledge. Our data also suggest that neutrophil-like monocytes may be functionally involved in human disease pathogenesis. Although the MS1 gene signature has been associated with bacterial infection (63) and risk of acute respiratory distress syndrome in severe sepsis (70), causality has not yet been established. Here, we demonstrate early evidence that the human MS1 monocyte population is analogous to the GMP-derived neutrophil-like monocyte in mice (Figure 8). By demonstrating that murine neutrophil-like monocytes recapitulate human MS1 monocytes and that murine neutrophil-like monocytes may be pathogenic, our data suggest that the clinical association of the MS1 signature with poor outcomes reflects an underlying causal role of MS1 monocytes in human disease. Future work will determine whether neutrophil-like monocytes are detrimental in lung injury, including the specific functions and alterations of these functions occurring after CLP.

A potentially novel observation arising from this work is that neutrophil-like monocytes may be pathogenic. Previous functional studies, though sparse, have demonstrated a protective role for GMP-derived neutrophil-like monocytes (34, 38, 59). Ly6C^{hi} monocytes expressing high levels of neutrophil granule genes and *Ym1* (chitinase-like 3, *Chil3*) are protective against experimental colitis (59) and brain injury (38) and display functions of MDSCs. In contrast, we show that post-sepsis murine neutrophil-like monocytes are associated with enhanced LPS-induced acute lung injury, and a similar neutrophil-like transcriptional signature is associated with poor outcomes in human sepsis (70). Interestingly, this contrasts with monocytes in acute lung injury without preceding sepsis, which are protective (14). Our results suggest that post-sepsis neutrophil-like monocytes may adopt an alternate inflammatory program without the protective features seen in colitis, brain injury, and lung injury without prior sepsis. This implies that the functions of GMP-derived or neutrophil-like monocytes in inflammatory organ injury may be heterogeneous and dependent on disease or tissue context, rather than GMP origin or neutrophil-like identity alone. However, this interpretation is complicated by a lack of consensus terminology and defining features of monocyte lineages and substates (e.g., GMP-monocyte, neutrophil-like, CD177^{+}-monocyte, *Ym1*-expressing) (71). By uncovering previously unappreciated complexity in monocyte heterogeneity, our study underscores the nascent state of this field and the need to harmonize observations of GMP-lineage and neutrophil-like monocytes across health and disease states to understand their functional heterogeneity.

These findings challenge our understanding of immune memory, suggesting that it may occur not only through epigenetic priming of proinflammatory genes, but also through reprogramming of hematopoietic progenitors toward alternate monocyte lineages. Innate immune memory, the durable reprogramming of immune progenitors for enhanced responses to secondary stimuli (55, 72, 73), may protect the host from secondary bacterial infections (72–74) but can be maladaptive in other inflammatory diseases (72, 75–77). Immune memory is established through alterations in chromatin accessibility at proinflammatory genes, induced by a primary stimulus, thereby facilitating transcription factor binding upon a secondary insult (25). Accordingly, we found that sepsis alters chromatin accessibility with enrichment of AP-1 motifs and enhanced JAK/STAT, HIF-1α, and TLR signaling, which are established mechanisms of immune

memory (10, 54, 55, 73, 78, 79). Thus, our findings suggest that innate immune memory contributes to monocyte pathogenicity in lung injury after sepsis; however, whether enhanced lung injury at 3 weeks and 3 months after sepsis occur through the same mechanisms, and specifically through neutrophil-like monocytes, remains to be determined. We also demonstrate that sepsis alters lineage specification, leading to expansion of GMPs and neutrophil-like monocytes in association with persistent low-grade G-CSF (Figure 7). Previous reports of immune memory have noted a myeloid differentiation bias in hematopoietic progenitors (55, 72, 73), and enhanced myelopoiesis could be a mechanism through which prior sepsis enhances secondary lung injury. However, additional literature hints that neutrophil-like monocyte expansion might be an aspect of in vivo innate immune memory (79, 80): our findings suggest this may reflect expansion of GMP-lineage monocytes and lingering G-CSF signaling. Alternatively, it may imply intrinsic GMP-lineage monocyte bias, as shown in a primate model of chronic alcohol exposure after weeks to months of abstinence, in which monocytes exhibit enhanced response to secondary stimuli and hematopoietic progenitors are biased toward production of neutrophil-like monocytes (80). These data suggest that immune memory may involve both altered inflammatory programming and shifts in ontogeny in monocyte progenitors, establishing a foundation for future studies to assess the role of altered monocyte ontogeny in immune memory in other contexts, the underlying mechanisms, and how shifts in ontogeny and trained immunity may interact to regulate monocyte function.

This study has some limitations. Although we establish that post-CLP monocytes are causal in enhanced lung injury in association with expansion of the neutrophil-like subset, we have not determined the soluble factors and specific causal role of neutrophil-like monocytes in enhanced lung injury. In addition, our approach cannot account for lung-intrinsic memory of prior sepsis, which may influence the response to prior inflammatory exposures. There are additional inherent limitations in our methodology such that adoptive transfer and depletion strategies could have off-target effects independent of monocytes or their direct functions in the lungs; transgenic approaches may be helpful to target monocytes in the future. Furthermore, our focus on acute time points limits our ability to extrapolate these observations to the resolution phase of lung injury. We utilized LPS to induce lung injury; future research on how post-sepsis monocyte reprogramming affects lung injury and host defense in the setting of live bacterial or viral infection is warranted, as post-sepsis priming of monocytes could have beneficial rather than detrimental effects in infectious contexts. Although we demonstrate that elevated monocyte counts and neutrophil counts concomitantly predict poor clinical outcomes in sepsis survivors, and our acute sepsis data suggest expansion of neutrophil-like monocyte orthologs in acute sepsis, further studies need to evaluate specific monocyte subsets in the circulation in patients who have survived sepsis. This will be crucial to completely understand durable immune reprogramming, shifts in ontogeny, and their long-term clinical consequences in human sepsis.

In summary, our findings provide insight into fundamental questions in the emerging field of monocyte heterogeneity (69): the extent to which Ly6C^{hi} monocyte subsets and inflammatory context regulate functional heterogeneity in health and disease. Our data suggest that Ly6C^{hi} monocytes enhance the lung injury response to LPS by promoting neutrophil degranulation. Moreover, we observed a functional role for neutrophil-like monocytes in the pathogenesis of acute lung injury. Although diverse functions of monocytes in different etiologies of acute lung injury (14–17, 19–21, 81–83) have supported the prevailing paradigm that their activation status and function are dictated by the local lung milieu (13), we demonstrate here that functional monocyte heterogeneity may also be shaped by the imprinting of monocyte progenitors in the BM by prior exposures leading to the expansion of specific monocyte subsets. The interplay between monocyte subsets and the local lung environment in shaping monocyte function across diverse etiologies of acute lung injury is an important topic for future research. With the discovery of a potentially subset-specific phenotype, these observations establish a foundation for future investigations to address key gaps in our understanding of how monocyte subset and prior inflammatory exposures might collaborate to enhance tissue injury responses. Studies of the functional role of specific monocyte subsets in the BM in lung injury, their selection by the lung inflammatory milieu, and their effect on the phenotype of recruited macrophages will help refine our prior understanding of monocyte/macrophage-mediated inflammation in the lungs. Finally, the persistent nature of hematopoietic reprogramming after sepsis in mice identifies a potential therapeutic target for the prevention of post-sepsis organ injury leading to rehospitalization in humans.

Methods

Sex as a biological variable. The patient cohort study included female patients. The animal studies were performed in male mice to limit sample size due to inter-animal variability in lung injury response because of prior sepsis. Sex as a biological variable was not evaluated in this study. We have found that female post-CLP mice have similarly enhanced lung injury, and prior studies have not shown sex-specific functions of monocytes in LPS-induced lung injury models, to our knowledge; as such, we expect the mechanisms to be broadly relevant to both sexes.

Mouse studies. Male 8- to 12-week-old C57BL/6J (strain 000664) and *Ccr2*$^{-/-}$ (strain 004999) mice were purchased from The Jackson Laboratory. Gfi1-tdTomato mice were obtained through a materials transfer agreement with Georges Lacaud, University of Manchester, Manchester, United Kingdom (84). All procedures involving animals were undertaken in strict accordance with the recommendations of the *Guide for the Care and Use of Laboratory Animals* (National Academies Press, 2011). The University of Michigan facility maintains a specific pathogen–free barrier environment.

CLP. CLP was performed as previously described (12, 85). Briefly, animal suffering and distress were minimized using analgesia with local lidocaine as well as anesthesia with ketamine and xylazine. Under aseptic conditions, a 1–2 cm laparotomy was performed. The cecum was ligated with a silk suture and punctured once through-and-through with a 19-gauge needle. The incision was closed with surgical clips. Imipenem/cilastatin (Merck, 0.5 mg/mouse in 200 μL of normal saline) and normal saline (0.5 mL) were administered s.c. to all CLP mice immediately after surgery. This method induces polymicrobial bacterial peritonitis with disseminated infection, an average mortality of 10%, and clearance of bacterial cultures within 5–7 days (12, 85, 86). By 3 weeks, there is no difference in weight between groups (12). We also did not observe any additional mortality during the 3-week to 3-month recovery period, and aerobic peritoneal cultures in 3-month post-CLP mice remained negative (data not shown).

LPS-induced lung injury. *E. coli* LPS (O111:B4, Sigma-Aldrich) was administered i.n. at predetermined time points (18 to 84 days) after CLP or in age-matched unoperated control mice. We utilized unoperated control mice because we previously established that sham surgery and unoperated control mice have similar lung injury responses to LPS at 3 weeks after surgery (12). Briefly, mice were anesthetized using ketamine and xylazine. LPS dissolved in sterile normal saline (50 μg, 1 μg/μL) was administered 25 μL per nostril. Mice were euthanized 24 or 72 hours after LPS administration. The University of Michigan policy for humane endpoints was followed.

Monocyte depletion. Monocyte depletion was performed using an anti-CCR2 antibody (clone MC-21) (87) or rat IgG2b isotype (clone LTF-2, Bio X Cell, or clone MC-67) administered (i.p., 40 μg) 4 days prior (day –4), 2 days prior (day –2), and at the time of LPS administration (day 0). MC-21 and MC-67 were provided by Dr. Matthias Mack (87). Treatments were randomized within cage. At 72 hours after LPS, post-CLP mice treated with anti-CCR2 antibody had less mononuclear cells (Diff-Quik) in the BAL than isotype-treated mice, indicating monocyte depletion. One cohort (out of 4 total depletions) showed instead elevated mononuclear cell counts in the BAL relative to the isotype-treated control for all mice; this was inconsistent with monocyte depletion and was excluded from analysis.

BM isolation and immunomagnetic monocyte isolation. BM was isolated from femurs and tibia of post-CLP mice (days 21 and 84) and age-matched control mice. Briefly, mice were euthanized with ketamine and xylazine. In a biological safety cabinet using sterile technique, hind legs were disarticulated and placed in RPMI with 10% FBS and 1% penicillin/streptomycin (P/S). Bones were cleaned and placed briefly into 100% ethanol. Bones were then cut on both ends and flushed with RPMI with 10% FBS and 1% P/S using a 27-gauge needle. Marrow was disaggregated and then passed through a 100 μm filter to remove debris. Cells were counted on a hemocytometer using trypan blue. BM from 2 hind legs was resuspended in 1 mL PBS supplemented with 1 mM EDTA and 2% FBS. Monocytes were then isolated using the EasySep Monocyte Isolation kit (STEMCELL Technologies) per the manufacturer's recommendations. This method consistently led to isolation of approximately 1×10^6 to 2×10^6 cells with 95% CCR2$^+$ monocytes (Supplemental Figure 15).

Monocyte adoptive transfer. Monocytes from post-CLP, unoperated, and *Ccr2*$^{-/-}$ control mice were isolated and pooled (n = 2–5 mice). *Ccr2*$^{-/-}$ recipient mice were anesthetized with ketamine and xylazine, and 1×10^6 monocytes were administered in 100–200 μL of PBS via tail vein injection. Mice then immediately received i.n. LPS to induce lung injury. Treatments were randomized within cage. Studies to confirm migration of adoptively transferred cells were performed using monocytes labeled with CellTracker Deep Red (Invitrogen) per the manufacturer's instructions.

Monocyte and neutrophil ex vivo culture. Monocytes were isolated from BM and immunomagnetically enriched as above. Monocytes from individual post-CLP and unoperated control mice were resuspended at 2.5×10^5 cells/mL in 2 mL DMEM with 10% FBS with LPS (1 μg/mL) in a 12-well plate and incubated for 5 hours at 37°C with 5% CO_2. Plates were removed and placed on ice, and supernatants were removed and centrifuged at 450*g* for 10 minutes at 4°C. Cell-free supernatants were stored at –20°C until use.

Neutrophils were isolated from BM as previously described (88). Briefly, whole BM was isolated from hind legs, red cells were lysed using ACK lysis buffer for 1 minute in 37°C, and cells were washed with RPMI with 10% FBS with1% P/S. A density gradient was created by layering 3 mL of each of the following: Histopaque 1119 (Sigma-Aldrich, density 1.119 g/mL), Histopaque 1077 (Sigma-Aldrich, density 1.077 g/mL), and whole BM from 2 hind legs in ice-cold PBS. Centrifugation was performed at 872*g* at room temperature without brake for 30 minutes. Neutrophils were collected from the Histopaque interface and washed twice with RMPI with 10% FBS with 1% P/S. Neutrophils from 6 naive mice were pooled. Cells were counted by trypan blue exclusion on a hemacytometer and purity was assessed to be more than 90% using Diff-Quik (Baxter) on cytospins. Neutrophils were resuspended at 5×10^6 cells/mL in DMEM with 10% FBS and transferred to wells containing 1 mL of thawed monocyte CM (post-CLP or control) or fresh basal media with or without LPS (1 μg/mL) in a 12-well plate. Cells were incubated for 5 hours at 37°C with 5% CO_2. Supernatants were isolated as above.

Serum collection and complete blood cell counts. Whole blood was obtained by puncture of the right ventricle using a heparinized 1 mL syringe and a 26-gauge needle. Needles were removed, and then blood was ejected and placed on ice for no more than 1 hour. Samples were centrifuged at 2000*g* for 10 minutes, with serum stored at –80°C until time of use. For complete blood cell counts, unheparinized whole blood was placed into EDTA Microtainer tubes (BD Biosciences). Blood counts were performed on a Hemavet HV950 (Drew Scientific) in the In-Vivo Animal Core at the University of Michigan.

BAL, cell count, and differential. Mice were euthanized with ketamine and xylazine. BAL was performed as described previously (12). The trachea was exposed and intubated using a 1.7 mm outer diameter polyethylene catheter. Active insufflation of PBS with 5 mM EDTA in 1 mL aliquots was performed, 3 times per mouse. BAL was centrifuged, supernatant removed, aliquoted, and stored at –80°C until further use. Cell pellets were resuspended and counted using trypan blue exclusion counting on a hemocytometer. Cytospins were prepared and stained with Diff-Quik (Baxter) to determine differential for polymorphonuclear nuclear and mononuclear cells.

Flow cytometry and cell sorting. BM or BAL cells were washed, blocked for non-specific staining with anti-CD16/32 Fc receptor block (clone 2.4G2, BD), and stained with fluorophore-conjugated antibodies prior to analysis on an Attune NxT (Thermo Fisher Scientific), MA900 (Sony), or FACSDiscover S8 (BD Biosciences) flow cytometer and cell sorter. For BM preparations, cells from a single femur and tibia were lineage depleted using streptavidin beads (STEMCELL Technologies) and biotinylated antibodies against TER-119, CD19, CD3e. Briefly, cells were resuspended in PBS with 1 mM EDTA and 2% FBS, blocked with 5% rat serum, and incubated with biotinylated antibodies for 5 minutes at room temperature. Lineage depletion was performed on an EasyEights EasySep magnet (STEMCELL Technologies) per protocol. In some studies evaluating BM progenitors, CD16/32 block was substituted with fluorophore-conjugated CD16/32 antibody. Antibodies included Ly6G (1A8, BioLegend), CD11b (M1/70, BioLegend), CD45 (30-F11, BioLegend), Ly6C (HK1.4, BioLegend), CD11c (N418, BioLegend), CD64 (X54-5/7.1.1, BD Biosciences), CD24 (M1/69, BD Biosciences), MHCII/I-A/E (clone M5/144.15.2, BioLegend), Siglec-F (E50-2440, BD Pharmingen), CD34 (HM34, BioLegend), CD115 (AFS98, BioLegend), CD135/Flt3 (A2-F10, BioLegend), CD117/c-kit (2B8, BioLegend), CD16/32 (93, BioLegend), and SlamF7 (4G2, BD Biosciences). Lineage markers included TER-119 (TER-119, BioLegend), CD3e (145-2C11, BioLegend), B220 (RA3-6B2, BioLegend), CD19 (eBIO1D3, eBioscience), and NK1.1 (PK136, BioLegend). For live/dead discrimination, 7-AAD was used. Selected populations were isolated by cell sorting 13,000–300,000 cells directly into TRIzol LS (Invitrogen) for RNA-Seq and 50,000–60,000 cells into PBS with 2% BSA (Thermo Fisher Scientific) for ATAC-Seq.

Quantification of BAL and supernatant proteins. BAL samples and supernatants were assayed for various proteins using the following ELISAs at dilutions where all samples were within the dynamic range of the standard curve: TNF-α, IL-1β, IL-6, MIP-2, MCP-1, KC, IL-1ra, S100A8/A9, and RAGE (Mouse DuoSet, R&D Systems); Pierce BCA assay (Thermo Fisher Scientific); and albumin (Bethyl Laboratories). Because of interexperiment variability in measurements over time, all protein values were expressed relative to the mean of contemporaneous controls for each cohort to preserve within-cohort effect sizes.

RNA isolation. RNA was isolated from monocyte and progenitor populations using TRIzol LS (Invitrogen) as described by the manufacturer. DNAse treatment was performed on RNeasy Mini kit columns (QIAGEN) prior to sequencing.

RNA-Seq, ATAC-Seq, and analysis. Sorted monocytes were subjected to bulk RNA-Seq and ATAC-Seq (see Supplemental Methods for more details). For RNA-Seq data, PCA was performed using prcomp, and a single outlier in the CLP group was excluded from analysis for a total of 4 CLP and 5 unoperated samples (Supplemental Figure 16).

Generation of monocyte subset gene signatures for monocytes and their progenitors. Gene sets for MDP- and GMP-derived monocyte-committed progenitors (MP and cMoP, respectively) and Ly6C^{hi} monocyte subsets (neutrophil-like and DC-like, respectively) were defined by a prior ex vivo experiment (33) and are available in the Genomic Data Supplement. To calculate the enrichment of monocyte and progenitor subset gene signature expression in sorted Ly6C^{hi} monocyte (Lin^{-}/Ly6G^{-}/CD115^{+}/CD11b^{hi}/Ly6C^{hi}/c-Kit^{-}/Flt3^{-}) and BM progenitors, gene expression data were normalized with *DESeq2* (v1.38.3), and the mean expression level of all genes in each signature was calculated for each sample and $\log_2$ transformed. A Wilcoxon's test was used to determine the difference between groups using *ggpubr* (v0.6.0).

Ex vivo monocyte subset cytokine secretion and phagocytosis response. Naive Gfi1-tdTomato mice were used to isolate the GMP-derived monocyte fraction (i.e., SlamF7^{neg}) (39). BM was collected and monocyte negative enrichment performed (STEMCELL Technologies) as above. Gfi1^{pos} and Gfi1^{neg} monocytes were sorted into PBS with 50% FBS (Supplemental Figure 11A). Monocytes were then resuspended (1×10^6 cells/mL) and assessed for various functions: (a) cytokine response to LPS (1 μg/mL in RPMI, 6 hours, 37°C) or (b) phagocytosis of *E. coli* bioparticles (Invitrogen,100 μg/mL, 1 hour, 37°C) per the manufacturer's instructions.

Ex vivo efferocytosis assessment. Thymocytes were isolated and labeled with CFSE (CellTrace) per the manufacturer's instructions. Apoptosis was induced with dexamethasone (5 μM in RPMI, 37°C overnight). Thymocytes were added in a 10:1 ratio to sorted monocyte subsets and incubated for 2 hours at 37°C. Efferocytosis was assessed by flow cytometry.

Human monocyte analysis. Human-mouse conserved monocyte subsets were defined using scRNA-Seq gene lists from mouse and human lung tumor (67) (See Genomic Data Supplement for detailed gene lists). Similarly, mouse-specific signatures were defined using mouse BM Ly6C^{hi} monocytes (36). Gene transcripts per million (TPM) were used from CD14^{+} monocytes from critically ill patients with sepsis (64) (GSE139913) and hospitalized patients with community acquired pneumonia (65) (GSE160329), and their respective healthy controls were acquired using the NCBI's Gene Expression Omnibus web client, GEO2R (https://www.ncbi.nlm.nih.gov/geo/geo2r/) accessed January 25, 2024. Human peripheral blood monocyte subsets (MS1–MS4) during acute bacterial infection were previously determined (63). This data was accessed and analyzed through the Single Cell Portal (Broad Institute; https://singlecell.broadinstitute.org/single_cell/study/SCP548/) accessed January 25, 2024, using the gene search and dot plot functions at default settings.

Proteomics data from CD14^{+} monocytes from patients with septic shock were downloaded from the PRIDE repository (PXD023938) (66). The dataset was acquired in data-dependent acquisition (DDA) mode. MS raw files were converted to mzML format using MSConvert from the ProteinWizard suite. The mzML files were analyzed with the FragPipe computational platform (v23) using the default LFQ_MBR workflow. MSFragger (89) (v.4.2) was used to search the data against the mouse reference proteome database from Uniprot (downloaded on April 22, 2025), appended with an equal number of reserved sequences and common contaminants. The search results were further processed using MSBooster (90) for deep learning–based rescoring; Percolator (91) for peptide-spectrum matches validation; ProteinProphet (92) for protein inference; and Philosopher (93) for FDR filtering at 1% FDR for PSM, peptide, and protein levels. The resulting files were passed to IonQuant (94) to extract and quantify peptides and proteins from the DDA data. The combined protein output file was used for downstream analysis. Only proteins with quantification values in 2 of 3 replicates per sample and present in at least 2 samples per condition were included for the final analysis. Certain proteins (e.g., IL-1R2) were only detected in healthy patients or those with sepsis, and imputation was performed for missing values using the lowest $\log_2$ protein abundance within the dataset. Enrichment for monocyte subset proteins was tested using MANOVA or PERMANOVA (if imputation performed) using the *stats* and *vegan* R packages between conditions.

Blood count analysis in patients surviving sepsis. The VA health care system provides comprehensive medical care to over 6 million veterans (95). During the study period, the VA used a single electronic health record system, archived in the Corporate Data Warehouse (CDW) and accessible for research (95).

Patient and hospitalization data, including demographics, comorbidities, and hospital treatments were extracted from the VA CDW, as described previously (62, 96). Sepsis hospitalizations with live discharge and relevant laboratory data were identified across 138 nationwide VA hospitals (2013 to 2018). Sepsis hospitalizations were identified using electronic health record data, as previously described (9, 62, 96–98). Specifically, we identified hospitalizations admitted through the (a) emergency department with evidence of (b) suspected infection and (c) acute organ dysfunction of 1 or more organs (97) with specific criteria available in Supplemental Table 2. Live discharge was defined as being alive on the calendar day of discharge and the day following (to exclude patients discharged home at end of life). We defined relevant laboratory data as having both AMC and ANC on the calendar day of discharge or day prior. Laboratory values were cleaned and standardized as previously described (9, 62). Nonphysiological laboratory values were excluded (Supplemental Table 3), and then the top and bottom 1% of the remaining values were excluded (Supplemental Table 4).

The association of each parameter with 90-day mortality was evaluated through fitting Cox proportional hazards models and restricted cubic splines using the R package *rms* (v6.0-0). To evaluate the effect of concomitant ANC on the association of AMC with 90-day mortality, the interaction between ANC and AMC was modeled using Cox proportional hazards, and the interaction surface was plotted using the R package *visreq* (v2.7.0). All statistical code is available online (https://github.com/CCMRPulmCritCare/MonocyteAnalysis; commit ID 78f9a06).

Statistics. Analyses included ANOVA followed by post hoc testing when ANOVA was significant or unpaired 2-tailed Student's *t* test as indicated in the text. A *P* value of less than 0.05 was considered statistically significant. In order to minimize spurious comparisons, we prespecified post hoc comparisons only between CLP/unoperated. Heatmaps were created using standardized *z* scores calculated by gene or protein across conditions. All figures show mean and standard error unless otherwise specified. Statistical analyses were carried out in GraphPad Prism (version 9).

Study approval. The patient cohort study was reviewed by the VA Ann Arbor IRBs and was deemed exempt from the need for consent under 45 CFR §46, category 4 (secondary use of identifiable data). The murine study protocol was approved by the IACUC of the University of Michigan (protocols 00008999 and 00010712).

Data availability. Figure-specific data is available in Supporting Data Values file. Transcriptomics and epigenomics data are available in NCBI's publicly accessible GEO (GSE268367 and GSE268368); please contact the corresponding author for other data. All code is available online (https://github.com/B-McBean/denstaedt_monocyte/tree; commit ID a95be80).

Manuscript information

Author contributions. SJD, APB, HCP, MM, BBM, HSG, and RLZ designed the study. SJD, JC, BCA, and MWN collected the data. SJD, APB, BM, HCP, HSG, YD, AIN, BHS, and RLZ analyzed and interpreted the data. SJD, HSG, and RLZ drafted the manuscript. All authors provided critical revision and approval of the final version of this manuscript.

AI disclosure. The authors declare use of AI for coding and data extraction for transcriptomics and proteomics analysis. AI model GPT-4o mini was used from April 2025 to August 2025.

Conflict of interest. AIN is the founder of Fragmatics and serves on the scientific advisory boards of Protai Bio, Infinitopes, and MOBILion Systems.

Funding. This study was supported by the following grants:

- National Heart, Lung, and Blood Institute (NHLBI) K08HL153799 (to SJD).
- National Human Genome Research Institute (NHGRI) U01HG011952 (to APB).
- NHGRI T32HG000040 (to BM).
- NHLBI R35HL144481 (to BBM).
- NIA R01AG074968 (to BHS).
- AHRQ R01HS026725 and VA HSR 20-313 (to HCP).
- National Institute of Allergy and Infectious Diseases R01AI134987 (to HSG).
- NHLBI R01HL147920, R01HL131608, and R35HL160770 (to RLZ).

This work is the result of NIH funding, in whole or in part, and is subject to the NIH Public Access Policy. Through acceptance of this federal funding, the NIH has been given a right to make the work publicly available in PubMed Central.

Acknowledgments. SJD would like to acknowledge Theodore J. Standiford for his support of the project concepts and Linda G. Denstaedt for her support.

Address for correspondence. Rachel L. Zemans, University of Michigan, 4063 Biomedical Science Research Building, 109 Zina Pitcher Pl., Ann Arbor, Michigan, 48103, USA. Phone: 734.936.7576; Email: zemansr@med.umich.edu.

1. Rudd KE, et al. Global, regional, and national sepsis incidence and mortality, 1990-2017: analysis for the Global Burden of Disease Study. *Lancet*. 2017;395(10219):200–211.
2. Prescott HC, et al. Readmission diagnoses after hospitalization for severe sepsis and other acute medical conditions. *JAMA*. 2015;313(10):1055–1057.
3. Prescott HC, et al. Late mortality after sepsis: propensity matched cohort study. *BMJ*. 2016;353:i2375.
4. Shankar-Hari M, et al. Rate and risk factors for rehospitalisation in sepsis survivors: systematic review and meta-analysis. *Intensive Care Med*. 2020;46(4):619–636.
5. Donnelly JP, et al. Readmission and death after initial hospital discharge among patients with COVID-19 in a large multihospital system. *JAMA*. 2021;325(3):304–306.
6. Prescott HC, Angus DC. Enhancing recovery from sepsis: a review. *JAMA*. 2018;319(1):62–75.
7. Yende S, et al. Inflammatory markers at hospital discharge predict subsequent mortality after pneumonia and sepsis. *Am J Respir Crit Care Med*. 2008;177(11):1242–1247.
8. Yende S, et al. Long-term host immune response trajectories among hospitalized patients with sepsis. *JAMA Netw Open*. 2019;2(8):e198686.
9. Denstaedt SJ, et al. Blood count derangements after sepsis and association with post-hospital outcomes. *Front Immunol*. 2023;14(february):1133351.
10. Cheong J gyu, et al. Epigenetic memory of coronavirus infection in innate immune cells and their progenitors. *Cell*. 2023;186(18):3882–3902.
11. Prescott HC, et al. Understanding and enhancing sepsis survivorship. Priorities for research and practice. *Am J Respir Crit Care Med*. 2019;200(8):972–981.
12. Denstaedt SJ, et al. Long-term survivors of murine sepsis are predisposed to enhanced LPS-induced lung injury and proinflammatory immune reprogramming. *Am J Physiol Lung Cell Mol Physiol*. 2021;321(2):L451–L465.
13. Herold S, et al. Acute lung injury: how macrophages orchestrate resolution of inflammation and tissue repair. *Front Immunol*. 2011;2:65.
14. Herold S, et al. Exudate macrophages attenuate lung injury by the release of IL-1 receptor antagonist in gram-negative pneumonia. *Am J Respir Crit Care Med*. 2011;183(10):1380–1390.
15. Herold S, et al. Lung epithelial apoptosis in influenza virus pneumonia: the role of macrophage-expressed TNF-related apoptosis-inducing ligand. *J Exp Med*. 2008;205(13):3065–3077.
16. Schmit T, et al. Interferon-γ promotes monocyte-mediated lung injury during influenza infection. *Cell Rep*. 2022;38(9):110456.
17. Cole SL, et al. M1-like monocytes are a major immunological determinant of severity in previously healthy adults with life-threatening influenza. *JCI Insight*. 2017;2(7):e91868.
18. Xiong H, et al. Innate lymphocyte/Ly6C(hi) monocyte crosstalk promotes Klebsiella pneumoniae clearance. *Cell*. 2016;165(3):679–689.
19. Xiong H, et al. Distinct contributions of neutrophils and CCR2^{+} monocytes to pulmonary clearance of different klebsiella pneumoniae strains. *Infect Immun*. 2015;83(9):3418–3427.
20. Jiang Z, et al. Depletion of circulating monocytes suppresses IL-17 and HMGB1 expression in mice with LPS-induced acute lung injury. *Am J Physiol Lung Cell Mol Physiol*. 2017;312(2):L231–L242.
21. Coates BM, et al. Inflammatory monocytes drive influenza A virus-mediated lung injury in juvenile mice. *J Immunol*. 2018;200(7):2391–2404.
22. Ifrim DC, et al. Trained immunity or tolerance: opposing functional programs induced in human monocytes after engagement of various pattern recognition receptors. *Clin Vaccine Immunol*. 2014;21(4):534–545.
23. Divangahi M, et al. Trained immunity, tolerance, priming and differentiation: distinct immunological processes. *Nat Immunol*. 2021;22(1):2–6.
24. Lachmandas E, et al. Microbial stimulation of different Toll-like receptor signalling pathways induces diverse metabolic programmes in human monocytes. *Nat Microbiol*. 2016;2(0):16246.
25. Dulfer EA, et al. Enduring echoes: post-infectious long-term changes in innate immunity. *Eur J Intern Med*. 2024;123(november):15–22.
26. Denstaedt SJ, et al. Sepsis and nosocomial infection: patient characteristics, mechanisms, and modulation. *Front Immunol*. 2018;9:2446.
27. Foster SL, et al. Gene-specific control of inflammation by TLR-induced chromatin modifications. *Nature*. 2007;447(7147):972–978.
28. Munoz C, et al. Dysregulation of in vitro cytokine production by monocytes during sepsis. *J Clin Invest*. 1991;88(5):1747–1754.
29. Hoogeveen RM, et al. Monocyte and haematopoietic progenitor reprogramming as common mechanism underlying chronic inflammatory and cardiovascular diseases. *Eur Heart J*. 2018;39(38):3521–3527.
30. Bekkering S, et al. In vitro experimental model of trained innate immunity in human primary monocytes. *Clin Vaccine Immunol*. 2016;23(12):926–933.
31. Quintin J, et al. Candida albicans infection affords protection against reinfection via functional reprogramming of monocytes. *Cell Host Microbe*. 2012;12(2):223–232.
32. Dominguez-Andres J, Netea MG. Long-term reprogramming of the innate immune system. *J Leukoc Biol*. 2018;105(2):329–338.

33. Yáñez A, et al. Granulocyte-monocyte progenitors and monocyte-dendritic cell progenitors independently produce functionally distinct monocytes. *Immunity*. 2017;47(5):890–902.
34. Ikeda N, et al. The early neutrophil-committed progenitors aberrantly differentiate into immunoregulatory monocytes during emergency myelopoiesis. *Cell Rep*. 2023;42(3):112165.
35. Weinreb C, et al. Lineage tracing on transcriptional landscapes links state to fate during differentiation. *Science*. 2020;367(6479):eaaw3381.
36. Barman PK, et al. Production of MHCII-expressing classical monocytes increases during aging in mice and humans. *Aging Cell*. 2022;21(10):e13701.
37. Ikeda N, et al. Emergence of immunoregulatory Ym1+Ly6Chi monocytes during recovery phase of tissue injury. *Sci Immunol*. 2018;3(28):eaat0207.
38. Gudenschwager Basso EK, et al. Immunoregulatory and neutrophil-like monocyte subsets with distinct single-cell transcriptomic signatures emerge following brain injury. *J Neuroinflammation*. 2024;21(1):41.
39. Trzebanski S, et al. Classical monocyte ontogeny dictates their functions and fates as tissue macrophages. *Immunity*. 2024;57(6):1225–1242.
40. Uchida T, et al. Receptor for advanced glycation end-products is a marker of type I cell injury in acute lung injury. *Am J Respir Crit Care Med*. 2006;173(9):1008–1015.
41. Rittirsch D, et al. Acute lung injury induced by lipopolysaccharide is independent of complement activation. *J Immunol*. 2010;180(11):7664–7672.
42. Reutershan J, et al. Critical role of endothelial CXCR2 in LPS-induced neutrophil migration into the lung. *J Clin Invest*. 2006;116(3):695–702.
43. Zarbock A, et al. Therapeutic inhibition of CXCR2 by Reparixin attenuates acute lung injury in mice. *Br J Pharmacol*. 2008;155(3):357–364.
44. Sheridan BC, et al. Neutrophils mediate pulmonary vasomotor dysfunction in endotoxin-induced acute lung injury. *J Trauma*. 1997;42(3):391–6; discussion 396.
45. Kawabata K, et al. Delayed neutrophil elastase inhibition prevents subsequent progression of acute lung injury induced by endotoxin inhalation in hamsters. *Am J Respir Crit Care Med*. 2000;161(6):2013–2018.
46. Sprenkeler EGG, et al. S100A8/A9 is a marker for the release of neutrophil extracellular traps and induces neutrophil activation. *Cells*. 2022;11(2):236.
47. Stroncek DF, et al. The subcellular distribution of myeloid-related protein 8 (MRP8) and MRP14 in human neutrophils. *J Transl Med*. 2005;3:36.
48. Sreejit G, et al. Neutrophil-derived S100A8/A9 amplify granulopoiesis after myocardial infarction. *Circulation*. 2020;141(13):1080–1094.
49. Simard JC, et al. Induction of neutrophil degranulation by S100A9 via a MAPK-dependent mechanism. *J Leukoc Biol*. 2010;87(5):905–914.
50. Asti C, et al. Lipopolysaccharide-induced lung injury in mice. I. Concomitant evaluation of inflammatory cells and haemorrhagic lung damage. *Pulm Pharmacol Ther*. 2000;13(2):61–69.
51. Mollinedo F. Neutrophil degranulation, plasticity, and cancer metastasis. *Trends Immunol*. 2019;40(3):228–242.
52. Ledderose C, et al. Optimized flow cytometry assays to monitor neutrophil activation in human and mouse whole blood samples. *J Immunol Methods*. 2023;512(december 2022):113403.
53. Sajti E, et al. Transcriptomic and epigenetic mechanisms underlying myeloid diversity in the lung. *Nat Immunol*. 2020;21(2):221–231.
54. Naik S, et al. Inflammatory memory sensitizes skin epithelial stem cells to tissue damage. *Nature*. 2017;550(7677):475–480.
55. Larsen SB, et al. Establishment, maintenance, and recall of inflammatory memory. *Cell Stem Cell*. 2021;28(10):1758–1774.
56. Naik S, Fuchs E. Inflammatory memory and tissue adaptation in sickness and in health. *Nature*. 2022;607(7918):249–255.
57. Watanabe H, et al. Single cell RNA-seq reveals cellular and transcriptional heterogeneity in the splenic CD11b+Ly6Chigh monocyte population expanded in sepsis-surviving mice. *Mol Med*. 2024;30(1):202.
58. Patel AA, et al. The fate and lifespan of human monocyte subsets in steady state and systemic inflammation. *J Exp Med*. 2017;214(7):1913–1923.
59. Ikeda N, et al. Emergence of immunoregulatory Ym1+Ly6Chi monocytes during recovery phase of tissue injury. *Sci Immunol*. 2018;3(28):1.
60. Yona S, et al. Fate mapping reveals origins and dynamics of monocytes and tissue macrophages under homeostasis. *Immunity*. 2013;38(1):79–91.
61. Yáñez A, Goodridge HS. Identification and isolation of oligopotent and lineage-committed myeloid progenitors from mouse bone marrow. *J Vis Exp*. 2018;137:58061.
62. Wang XQ, et al. Veterans Affairs patient database (VAPD 2014–2017): building nationwide granular data for clinical discovery. *BMC Med Res Methodol*. 2019;19(1):94.
63. Reyes M, et al. An immune-cell signature of bacterial sepsis. *Nat Med*. 2020;26(3):333–340.
64. Liepelt A, et al. Differential gene expression in circulating $CD14^+$ monocytes indicates the prognosis of critically ill patients with sepsis. *J Clin Med*. 2020;9(1):1.
65. Brands X, et al. An epigenetic and transcriptomic signature of immune tolerance in human monocytes through multi-omics integration. *Genome Med*. 2021;13(1):131.
66. de Azambuja Rodrigues PM, et al. Proteomics reveals disturbances in the immune response and energy metabolism of monocytes from patients with septic shock. *Sci Rep*. 2021;11(1):15149.
67. Zilionis R, et al. Single-cell transcriptomics of human and mouse lung cancers reveals conserved myeloid populations across individuals and species. *Immunity*. 2019;50(5):1317–1334.
68. Trzebanski S, Jung S. Plasticity of monocyte development and monocyte fates. *Immunol Lett*. 2020;227:66–78.
69. Wolf AA, et al. The ontogeny of monocyte subsets. *Front Immunol*. 2019;10:1642.
70. Leite GGF, et al. Monocyte state 1 (MS1) cells in critically ill patients with sepsis or non-infectious conditions: association with disease course and host response. *Crit Care*. 2024;28(1):88.

71. Mildner A, Yona S. Monocytes and their doppelgängers: An immunological crossroads. *Sci Immunol*. 2024;9(101):eadr6672.
72. Jentho E, et al. Trained innate immunity, long-lasting epigenetic modulation, and skewed myelopoiesis by heme. *Proc Natl Acad Sci U S A*. 2021;118(42):1.
73. de Laval B, et al. C/EBPβ-dependent epigenetic memory induces trained immunity in hematopoietic stem cells. *Cell Stem Cell*. 2020;26(5):657–674.
74. Kalafati L, et al. Innate immune training of granulopoiesis promotes anti-tumor activity. *Cell*. 2020;183(3):771–785.
75. Li X, et al. Maladaptive innate immune training of myelopoiesis links inflammatory comorbidities. *Cell*. 2022;185(10):1709–1727.
76. Haacke N, et al. Innate immune training of osteoclastogenesis promotes inflammatory bone loss in mice Innate immune training of osteoclastogenesis promotes inflammatory bone loss in mice. *Dev Cell*. 2025;60(13):1854–1870.
77. Rehill AM, et al. Trained immunity causes myeloid cell hypercoagulability. *Sci Adv*. 2025;11(10):eads0105.
78. Cheng SC, et al. mTOR- and HIF-1 -mediated aerobic glycolysis as metabolic basis for trained immunity. *Science*. 2014;345(6204):1250684.
79. Li W, et al. A single-cell view on host immune transcriptional response to in vivo BCG-induced trained immunity. *Cell Rep*. 2023;42(5):112487.
80. Lewis SA, et al. Integrated single cell analysis shows chronic alcohol drinking disrupts monocyte differentiation in the bone marrow. *Stem Cell Reports*. 2023;18(9):1884–1897.
81. Dhaliwal K, et al. Monocytes control second-phase neutrophil emigration in established lipopolysaccharide-induced murine lung injury. *Am J Respir Crit Care Med*. 2012;186(6):514–524.
82. Günes Günsel G, et al. The arginine methyltransferase PRMT7 promotes extravasation of monocytes resulting in tissue injury in COPD. *Nat Commun*. 2022;13(1):1303.
83. Puchta A, et al. TNF drives monocyte dysfunction with age and results in impaired anti-pneumococcal immunity. *PLoS Pathog*. 2016;12(1):e1005368.
84. Thambyrajah R, et al. GFI1 proteins orchestrate the emergence of haematopoietic stem cells through recruitment of LSD1. *Nat Cell Biol*. 2016;18(1):21–32.
85. Denstaedt SJ, et al. S100A8/A9 drives neuroinflammatory priming and protects against anxiety-like behavior after sepsis. *J Immunol*. 2018;200(9):3188–3200.
86. Dickson RP, et al. Enrichment of the lung microbiome with gut bacteria in sepsis and the acute respiratory distress syndrome. *Nat Microbiol*. 2016;1(10):16113.
87. Mack M, et al. Expression and characterization of the chemokine receptors CCR2 and CCR5 in mice. *J Immunol*. 2001;166(7):4697–4704.
88. Swamydas M, et al. Isolation of mouse neutrophils. *Curr Protoc Immunol*. 2015;110:3.20.1–3.20.15.
89. Kong AT, et al. MSFragger: ultrafast and comprehensive peptide identification in mass spectrometry-based proteomics. *Nat Methods*. 2017;14(5):513–520.
90. Yang KL, et al. MSBooster: improving peptide identification rates using deep learning-based features. *Nat Commun*. 2023;14(1):4539.
91. Käll L, et al. Semi-supervised learning for peptide identification from shotgun proteomics datasets. *Nat Methods*. 2007;4(11):923–925.
92. Nesvizhskii AI, et al. A statistical model for identifying proteins by tandem mass spectrometry. *Anal Chem*. 2003;75(17):4646–4658.
93. da Veiga Leprevost F, et al. Philosopher: a versatile toolkit for shotgun proteomics data analysis. *Nat Methods*. 2020;17(9):869–870.
94. Yu F, et al. IonQuant enables accurate and sensitive label-free quantification with FDR-controlled match-between-runs. *Mol Cell Proteomics*. 2021;20:100077.
95. Fihn SD, et al. Insights from advanced analytics at the Veterans Health Administration. *Health Aff (Millwood)*. 2014;33(7):1203–1211.
96. Vincent BM, et al. Using Veterans Affairs corporate data warehouse to identify 30-day hospital readmissions. *Health Serv Outcomes Res Methodol*. 2018;18(3):143–154.
97. Wayne MT, et al. Measurement of sepsis in a national cohort using three different methods to define baseline organ function. *Ann Am Thorac Soc*. 2021;18(4):648–655.
98. Wayne MT, et al. Temporal trends and hospital variation in time-to-antibiotics among veterans hospitalized with sepsis. *JAMA Netw Open*. 2021;4(9):e2123950.